Structural basis of ion permeation gating in Slo2.1 K^+ channels

Priyanka Garg,[1,2] Alison Gardner,[1] Vivek Garg,[1] and Michael C. Sanguinetti[1,3]

[1]Nora Eccles Harrison Cardiovascular Research and Training Institute, [2]Department of Pharmaceutics and Pharmaceutical Chemistry, and [3]Department of Internal Medicine, University of Utah, Salt Lake City, UT 84112

The activation gate of ion channels controls the transmembrane flux of permeant ions. In voltage-gated K^+ channels, the aperture formed by the S6 bundle crossing can widen to open or narrow to close the ion permeation pathway, whereas the selectivity filter gates ion flux in cyclic-nucleotide gated (CNG) and Slo1 channels. Here we explore the structural basis of the activation gate for Slo2.1, a weakly voltage-dependent K^+ channel that is activated by intracellular Na^+ and Cl^-. Slo2.1 channels were heterologously expressed in *Xenopus laevis* oocytes and activated by elevated $[NaCl]_i$ or extracellular application of niflumic acid. In contrast to other voltage-gated channels, Slo2.1 was blocked by verapamil in an activation-independent manner, implying that the S6 bundle crossing does not gate the access of verapamil to its central cavity binding site. The structural basis of Slo2.1 activation was probed by Ala scanning mutagenesis of the S6 segment and by mutation of selected residues in the pore helix and S5 segment. Mutation to Ala of three S6 residues caused reduced trafficking of channels to the cell surface and partial (K256A, I263A, Q273A) or complete loss (E275A) of channel function. P271A Slo2.1 channels trafficked normally, but were nonfunctional. Further mutagenesis and intragenic rescue by second site mutations suggest that Pro271 and Glu275 maintain the inner pore in an open configuration by preventing formation of a tight S6 bundle crossing. Mutation of several residues in S6 and S5 predicted by homology modeling to contact residues in the pore helix induced a gain of channel function. Substitution of the pore helix residue Phe240 with polar residues induced constitutive channel activation. Together these findings suggest that (1) the selectivity filter and not the bundle crossing gates ion permeation and (2) dynamic coupling between the pore helix and the S5 and S6 segments mediates Slo2.1 channel activation.

INTRODUCTION

Large conductance, K^+-selective channels activated by intracellular Na^+ (K_{Na} channels) are expressed in neurons (Bader et al., 1985; Haimann and Bader, 1989; Haimann et al., 1990, 1992; Egan et al., 1992; Dryer, 1994; Zhainazarov and Ache, 1997) and cardiac myocytes (Kameyama et al., 1984; Rodrigo and Chapman, 1990; Sanguinetti, 1990). K_{Na} channels recorded from excised inside-out patches are activated by elevated $[Na^+]_i$ with an EC_{50} that varies from 35 to 80 mM depending on experimental conditions (Kameyama et al., 1984; Yan et al., 2012). Thus, K_{Na} channels are expected to be predominantly in a closed state under normal physiological conditions ($[Na^+]_i$ = 5–10 mM) unless activated by a persistent inward sodium current (Budelli et al., 2009; Hage and Salkoff, 2012) or when $[Na^+]_i$ is transiently elevated during bursts of neuronal activity (Wendt-Gallitelli et al., 1993). In the heart, elevated $[Na^+]_i$ during severe ischemia results in activation of cardiac K_{Na} channels that shortens action potential duration (Kameyama et al., 1984; Sanguinetti, 1990; Wang et al., 1991) and prevents Ca^{2+} overload. In this manner, K_{Na} channels could serve a protective role in the heart similar to that proposed for ATP depletion–sensitive K^+ (K_{ATP}) channels. Indirect evidence suggests that Slo2 channels may also be expressed in the mitochondria and have a cytoprotective role (Wojtovich et al., 2011).

Two genes are known to encode K_{Na} channels. Both *Slick* ("sequence like an intermediate conductance K^+" channel) and *Slack* ("sequence like a calcium-activated K^+" channel; Bhattacharjee et al., 2003; Yuan et al., 2003) are most closely related to *Slo1* (Adelman et al., 1992), the large conductance Ca^{2+}-activated K^+ (BK) channel gene. Because of their homology to Slo1, Slick and Slack were subsequently given the names Slo2.1 and Slo2.2, respectively. Heterologous expression of Slo2.1 revealed that in addition to intracellular Na^+, these channels are also activated by intracellular Cl^- and NAD^+ (Tamsett et al., 2009), and inhibited by intracellular ATP (Bhattacharjee et al., 2003). Independent of changes in $[Ca^{2+}]_i$ or $[Na^+]_i$, both Slo1 (Ottolia and Toro, 1994) and Slo2.1 channels (Dai et al., 2010; Garg and Sanguinetti, 2012) can be activated by high concentrations of fenamates such as niflumic acid (NFA) and flufenamic acid.

Correspondence to Michael C. Sanguinetti: sanguinetti@cvrti.utah.edu

Abbreviations used in this paper: CNG, cyclic-nucleotide gated; GAPDH, glyceraldehyde 3-phosphate dehydrogenase; NFA, niflumic acid; $PI(4,5)P_2$ diC8, phosphatidylinositol 4,5-bisphosphate diC8.

The Rockefeller University Press $30.00
J. Gen. Physiol. Vol. 142 No. 5 523–542
www.jgp.org/cgi/doi/10.1085/jgp.201311064

For most voltage-gated K^+ (Kv) channels, the activation gate is formed by the criss-crossing of the intracellular ends of the four S6 segments, the so-called "bundle crossing" (Doyle et al., 1998). When the membrane is depolarized, the primary voltage sensors (S4 segments) of a Kv channel are outwardly displaced, and this movement is coupled to channel opening, a widening of the aperture formed by the S6 bundle crossing. In cyclic-nucleotide gated (CNG) channels, the aperture formed by the S6 bundle crossing also widens in response to cAMP or cyclic guanosine monophosphate (cGMP) interaction with the cytoplasmic cyclic nucleotide binding domain (CNBD; Flynn and Zagotta, 2001; Craven et al., 2008). However, pore block by intracellular Ag^+ (Flynn and Zagotta, 2001) or quaternary ammonium compounds (Contreras and Holmgren, 2006) is not dependent on the state of the channel, which suggests that the intracellular ends of the S6 segments do not form a bundle crossing to gate ion permeation. Instead, studies using substituted cysteine accessibility method (SCAM) indicate that a conformational change in the selectivity filter is associated with activation of ion permeation in CNG channels (Sun et al., 1996; Becchetti and Roncaglia, 2000; Liu and Siegelbaum, 2000; Contreras and Holmgren, 2006; Contreras et al., 2008). Together these findings imply that cyclic nucleotide binding to the CNBD is allosterically coupled via the S6 segments to a conformational change in the selectivity filter that opens the channel. Wilkens and Aldrich (2006) speculated that the selectivity filter also gates K^+ permeation in Slo1 channels because intracellular application of a quaternary ammonium compound (bbTBA) blocked both the open and closed state, which indicates that its access to the central cavity of the channel pore was not prevented by the bundle crossing. A SCAM approach was also used to conclude that the bundle crossing does not gate K^+ conductance in Slo1 channels (Zhou et al., 2011), or the small conductance calcium-gated potassium channels $K_{Ca2.2}$ (Bruening-Wright et al., 2007) and $K_{Ca3.1}$ (Klein et al., 2007). More recently, Chen and Aldrich (2011) postulated that subtle movements of the S6 segments are associated with Slo1 channel gating. They mutated the S6 residue Met314 to His, titrated its protonation state by varying pH (or mutated Met314 to a charged residue), and found that the open state of Slo1 was stabilized when the side chain of residue 314 was charged and presumably faced toward the pore. Based on these findings, Chen and Aldrich (2011) concluded that the S6 segments undergo a rearrangement during channel activation and deactivation, and that this structural change is manifested as a change in the extent to which residue 314 is exposed to the water-filled central cavity.

Here we use two experimental approaches to show that the main features of Slo2.1 channel gating resemble that previously described for CNG and Slo1 channels. First, we demonstrate that inhibition of Slo2.1 by verapamil and its quaternary derivative D890 is not open-channel dependent, implying that the S6 bundle crossing does not restrict drug access to the central pore. Second, scanning mutagenesis of the S6 segment and directed mutagenesis of the S5 segment and pore helix identified several residues critical for normal channel gating. Together our findings indicate that the selectivity filter, not the S6 bundle crossing, serves as the primary activation gate that controls ion permeation in Slo2.1 channels.

MATERIALS AND METHODS

Molecular biology

Human *Slo2.1* (*KCNT2*; NCBI Genbank accession no. NM_198503) cDNA in pTRACER plasmid (provided by L. Kaczmarek, Yale University, New Haven, CT) was isolated by EcoRV and SpeI digestion and subcloned into the psGEM oocyte expression vector. The QuikChange site-directed mutagenesis kit (Agilent Technologies) was used to introduce mutations into WT *Slo2.1* cDNA. Purified mutant cDNAs were sequenced by the University of Utah sequencing core facility. Plasmids were linearized with SfiI, and cRNA was prepared using the mMessage mMachine T7 kit (Ambion). Concentrations of cRNA were measured by using the RiboGreen RNA quantitation kit (Invitrogen).

Oocyte isolation and cRNA injection

Methods for anesthetizing adult female *Xenopus laevis* (immersion in 0.2% tricaine methanesulfonate solution) and surgical removal of ovarian lobes were approved by the University of Utah Institutional Animal Care and Use Committee. To isolate individual oocytes free of follicle cells, dispersed ovarian lobes were placed into a Ca^{2+}-free saline solution containing 2 mg/ml each of type I and II collagenase (Worthington Biochemical Corporation) and gently shaken for 1–1.5 h. The Ca^{2+}-free saline solution contained (in mM): 96 NaCl, 2 KCl, 1 $MgCl_2$, and 5 HEPES; pH was adjusted to 7.6 with NaOH. Stage IV and V oocytes were injected with a variable amount (0.2–10 ng, indicated in the figure legends) of WT or mutant *Slo2.1* cRNA, then incubated at 18°C for 1–7 d in Barth's saline solution that contained (in mM): 88 NaCl, 1 KCl, 0.41 $CaCl_2$, 0.33 $Ca(NO_3)_2$, 1 $MgSO_4$, 2.4 $NaHCO_3$, 10 HEPES, and 1 pyruvate plus gentamycin (50 mg/L); pH was adjusted to 7.4 with NaOH.

Two-electrode voltage-clamp protocols and data analysis

Ionic currents were recorded at room temperature (22–24°C) using standard two-microelectrode voltage-clamp techniques (Goldin, 1991; Stühmer, 1992). Oocytes were placed in a 0.3-ml oocyte chamber (RC-1Z; Warner Instruments) and superfused at a rate of ~2 ml/min with KCM211 solution that contained (in mM): 98 NaCl, 2 KCl, 1 $CaCl_2$, 1 $MgCl_2$, and 5 mM HEPES; pH adjusted to 7.6 with NaOH. In some experiments, this solution was modified to make K104 solution by increasing [KCl] to 104 mM and omitting NaCl. To reduce leakage of KCl from recording micropipettes into the oocytes, 1% agarose-cushion microelectrodes were fabricated as described previously (Schreibmayer et al., 1994). The tip resistances of agarose cushion microelectrodes ranged from 0.2–0.9 MΩ after back-filling with 3 M KCl. A GeneClamp 500 amplifier, Digidata 1322A data acquisition system, and pCLAMP 8.2 or 9.0 software (Molecular Devices) were used to produce command voltage steps and to record digitized current and voltage signals.

In most experiments, Slo2.1 current ($I_{Slo2.1}$) was activated with NFA (Sigma-Aldrich). NFA was prepared as a 1-M stock solution in dimethyl sulfoxide and stored at −20°C. The effect of NFA on uninjected cells was routinely determined for each batch of isolated oocytes. At concentrations up to 1 mM, NFA slightly reduced the magnitude of the small endogenous currents present in uninjected oocytes. However, at high concentration (>6 mM), NFA enhanced endogenous currents; e.g., from ∼0.2–0.5 µA to 1–3 µA at +80 mV. To record $I_{Slo2.1}$, voltage pulses were usually applied from a holding potential (V_h) of −80 mV to a test potential (V_t) that was varied in 20-mV increments from +80 to −140 mV. Unless specified otherwise, the interpulse interval was 10 s. In some experiments, Slo2.1 channels were activated by increasing $[NaCl]_i$ by filling the recording micropipettes with a 2.4 M NaCl solution. In the absence of an agarose plug, these electrodes had a resistance of 0.3–0.8 MΩ, and leakage of NaCl out of the pipette and into the oocyte quickly activated $I_{Slo2.1}$, reaching a peak effect in 5–7 min. This method of activating Slo2.1 channels proved useful as a secondary assay for functional expression of mutant channels, but has several obvious limitations, including uncertainty regarding $[NaCl]_i$ achieved and presumed preferential activation of channels located in the region of plasma membrane nearest to the electrode tips.

The conductance–voltage relationship for oocytes bathed in K104 solution was determined by plotting $I_{Slo2.1}/(V_t - E_{rev})$ as a function of V_t. The normalized conductance (G/G_{max}) was plotted as a function of V_t and fitted to a Boltzmann function (see the following equation), where z is the effective valence, F is Faraday's constant, R is the gas constant, T is room temperature in Kelvin, and $V_{0.5}$ is the potential at which $I_{Slo2.1}$ is half-activated: $G/G_{max} = 1/\{1 + \exp[-zF/RT(V_t - V_{0.5})]\}$.

To determine the cumulative [NFA]–response relationship, $I_{Slo2.1}$ was elicited with repetitive test pulses to 0 mV until the current (I) reached a steady-state level at each concentration of NFA. I/I_{max} was plotted as a function of [NFA] and the data were fitted with the logistic equation (see the following equation), where $I_{c\text{-}rel}$ represents constitutive $I_{Slo2.1}$ in the absence of NFA expressed as a fraction of maximally activated current, EC_{50} is the [NFA] that produced a half-maximal effect, and n_H is the Hill coefficient: $I / I_{max} = 1 + \left(I_{c\text{-}rel} - 1\right) / \left(\left[\text{NFA}\right] / EC_{50}\right)^{n_H}$.

The block of Slo2.1 channels by verapamil was determined by comparing $I_{Slo2.1}$ activated by 1 mM NFA applied before and after incubation of an oocyte with verapamil. The increase in $I_{Slo2.1}$ by NFA was monitored during repetitive pulsing to 0 mV from a holding potential of −90 mV. As soon as peak activation was achieved, NFA was washed out of the oocyte recording chamber until $I_{Slo2.1}$ was again undetectable. Verapamil was then added to the chamber for 10 min while the oocyte was clamped at a V_h of −90 mV without pulsing. After this equilibration period, the perfusate was switched to a solution containing verapamil plus 1 mM NFA as pulsing to 0 mV was resumed. The procedure was repeated once more with a higher concentration of verapamil. Currents were normalized to NFA-activated $I_{Slo2.1}$ under control conditions, and the mean data were fitted with the logistic equation to determine the IC_{50} for verapamil.

Macropatch recordings

The excised inside-out (I/O) configuration of the patch clamp technique (Hamill et al., 1981) was used to record $I_{Slo2.1}$ in macropatches of plasma membrane pulled from oocytes. The vitelline membrane from each oocyte was manually removed after treatment with hypertonic solution (300 mM sucrose) for 2–6 min. Patch pipettes were fabricated from 1 mm OD borosilicate glass capillaries (catalog No. BF150-86-15; World Precision Instruments) using a Sutter Instruments P-97 puller (Novato). After pulling, pipette tips were heat polished and had a resistance of 1–3 MΩ when filled with a pipette (extracellular) solution that contained (in mM): 98 NaCl, 2 KCl, 1 $CaCl_2$, 1 $MgCl_2$, and 10 HEPES; pH was adjusted to 7.2 with NaOH. NFA (2 mM) was also added to the pipette solution to activate Slo2.1. The bath (intracellular) solution contained (in mM): 98 KCl, 2 NaCl, 2 EGTA, 2 $MgCl_2$, and 10 HEPES; pH was adjusted to 7.2 with KOH. Recordings were made at room temperature (22–24°C) 4–7 d after oocytes were injected with 10–16 ng of cRNA. During preliminary studies, we observed a rapid time-dependent reduction ("run-down") of macroscopic $I_{Slo2.1}$ in excised patches that was preventable by application of 10 µM phosphatidylinositol 4,5-bisphosphate diC8 ($PI(4,5)P_2$ diC8) to the bath (cytosolic) solution. A feedback patch clamp amplifier (Axopatch 200B amplifier), a data acquisition system (Digidata 1322A), and pCLAMP 9.0 software (all from Molecular Devices) were used to produce command voltage steps and to record currents digitized at 5 kHz after on-line filtering at 1 kHz with an eight-pole low-pass Bessel filter. Macropatch currents were evoked during voltage ramps. From a V_h of −80 mV, a 160 ms prepulse to +80 mV was followed by a 1-s voltage ramp from +80 to −140 mV. The protocol was repeated every 5 s to monitor time-dependent changes and the effect of exposure to 100 µM verapamil or D890.

Data analysis

pCLAMP 9 software (Molecular Devices) was used to analyze digitized data. Origin 8.5 (OriginLab) was used for curve fitting and to prepare figures. All data are expressed as mean ± SEM (n = number of oocytes), and statistical significance was evaluated by a Student's t test where appropriate ($P \leq 0.05$ was considered a statistically significant difference).

Biotinylation and Western blot analysis

Biotinylation of oocytes was performed using a method similar to that described previously (Garg et al., 2012). Oocytes (80–90) were individually injected with WT *hSlo2.1* cRNA (1 or 10 ng) or 10 ng of mutant *hSlo2.1* cRNA and incubated in Barth's saline solution at 18°C. For these experiments, hSlo2.1 contained a C-terminal FLAG epitope tag. 3 d after injection, cells were first washed with ice-cold Ca^{2+}-free ND96 solution before cell surface proteins were labeled by incubation with Sulfo-NHS-SS-Biotin (1 mg/ml in KCM211) at 4°C. The biotinylation reaction was stopped after 1 h by the addition of quenching solution. Oocytes were then washed twice with KCM211 and Tris-buffered saline and lysed by 15-min incubation on ice with 500 µl of lysis buffer plus protease inhibitor. The buffer volume was increased up to 1 ml after homogenization and incubated for 15 min on ice, and the lysate was then centrifuged at 10,000 *g* for 10 min at 4°C. To isolate the cell surface proteins, clear supernatant was dialyzed against Avidin neutralized on beads (Thermo Fisher Scientific) for 2 h at 4°C. Thereafter, the beads were collected by centrifugation at 3,000 *g* for 2 min and washed four times with lysis buffer. After the final wash, the bound protein was eluted by incubating the beads with SDS-PAGE sample buffer containing 50 mM DTT at 60°C for 20 min. Protein samples from both the biotinylated membrane and cytosolic fractions were separated by SDS-PAGE electrophoresis and analyzed by a Western blotting technique using 1:2,000 dilution of mouse anti-FLAG primary antibody (Takara Bio Inc.) and a 1:7,500 dilution of horseradish peroxidase–conjugated goat anti–mouse secondary antibody. Samples were also analyzed for Na^+/K^+ ATPase (plasma membrane marker) with a 1:2,000 dilution of mouse primary antibody (Abcam) and a 1:5,000 dilution of anti–mouse secondary antibody. Glyceraldehyde 3-phosphate dehydrogenase (GAPDH; cytosolic marker) was detected with a 1:10,000 dilution of mouse primary antibody (Abcam) and a 1:5,000 dilution of goat anti–mouse antibody. All secondary antibodies were purchased from Jackson ImmunoResearch Laboratories, Inc. Densitometric analysis of Western blots developed for 15 min

was performed using ImageJ analysis software, and intensities of FLAG-tagged Slo2.1 protein bands were normalized to Na^+/K^+ ATPase protein bands.

Chemicals

D890 was purchased from Abcam. $PI(4,5)P_2$ diC8 was purchased from Echelon Biosciences Inc. All other drugs and chemicals were purchased from Sigma-Aldrich. $PI(4,5)P_2$ diC8 was stored as 150 µM stock in bath solution at −80°C in glass vials. Final drug solutions were prepared immediately before use by dilution of stock solutions stored at −20°C.

Molecular modeling

A homology model of the pore region (S5-PH-S6) of Slo2.1 based on the x-ray crystal structure of the open state MthK bacterial K^+ channel (PDB accession no. 1LNQ) was prepared using YASARA, version 13.6 (Krieger et al., 2002). Energy minimization was performed using the YASARA force field (Krieger et al., 2009).

RESULTS

State-independent pore block of Slo2.1 channels by verapamil and D890

The phenylalkylamine verapamil is known as a potent open channel blocker of voltage-gated Ca^{2+} channels (Lee and Tsien, 1983), but at higher concentrations it also blocks the open state of delayed rectifier K^+ channels (DeCoursey, 1995; Catacuzzeno et al., 1999; Zhang et al., 1999) and large conductance Ca^{2+}-activated K^+ (BK) channels (Harper et al., 2001). Verapamil is a weak base (pKa ∼9) and is thus largely protonated at physiological pH. Only the neutral form of the drug diffuses across the cell membrane into the cytoplasm where at steady-state it also exists mainly in a protonated state. Presumably, when channels are in their closed state, the narrow aperture formed by the S6 bundle crossing prevents protonated verapamil from gaining access to its binding site in the central cavity; when the channel is opened, the aperture is wide enough for these large drugs to enter the central pore and physically block the transmembrane flux of permeant ions. Furthermore, a permanently charged analogue of verapamil, D890, only blocks channels when applied to the cytoplasmic side of inside-out macropatches (DeCoursey, 1995; Kurokawa et al., 1997; Catacuzzeno et al., 1999; Harper et al., 2001). As verapamil and D890 have proved useful compounds to probe the state-dependent status of the S6 bundle crossing (open or closed) of diverse channel types, we characterized the effects of these drugs on Slo2.1.

$I_{Slo2.1}$ was not activated by depolarizing pulses in oocytes injected with ≤1 ng of WT *Slo2.1* cRNA. However, when oocytes were superfused with KCM211 solution containing NFA, $I_{Slo2.1}$ was activated immediately and increased in magnitude during repetitive pulsing until a peak response was obtained in ∼3 min (Fig. 1 A, *i*). For these experiments, 6 mM NFA was used to maximally activate WT Slo2.1 (Dai et al., 2010). When $I_{Slo2.1}$ reached a steady-state level, the perfusate was switched back to control solution to wash out NFA. Outward current gradually diminished as channels returned to a nonactivated closed state. Pulsing was then halted for 10 min as KCM211 solution containing 100 µM verapamil was perfused into the bath. Preliminary experiments determined that 10 min was sufficient time for channel block to reach a steady-state level. Pulsing to 0 mV was resumed as the oocyte was superfused with a solution containing 6 mM NFA plus 100 µM verapamil. The peak $I_{Slo2.1}$ activated by this second application of NFA was decreased by >90% (Figs. 1 A, *ii*; and Fig. 1 B). The same experimental protocol was repeated in another oocyte using *N*-methyl verapamil (D890), a permanently charged, membrane impermeant analogue of verapamil. Unlike verapamil, extracellular application of 100 µM D890 for 10 min did not reduce the magnitude of $I_{Slo2.1}$ during the second application of NFA (Fig. 1, C and D). Thus, D890 did not block Slo2.1 channels when applied to the extracellular solution. The experiments with verapamil or D890 were repeated in several oocytes and the mean results are presented in Fig. 1 E. To test for sidedness of block by the phenylalkylamines, currents were recorded from excised inside-out macropatches as voltage ramps from +80 to −140 mV were repetitively applied in the absence and presence of 100 µM verapamil (Fig. 1 F) or D890 (Fig. 1 G) in the bath solution. Both compounds caused nearly complete block of $I_{Slo2.1}$ in <1 min. Together these findings indicate that similar to Ca^{2+} and Kv channels, phenylalkylamines block Slo2.1 channels from the cytoplasmic side of the cell membrane, but contrary to these voltage-gated channels, verapamil blocked Slo2.1 channels that were in a nonconducting state.

State-dependence of verapamil block was also assessed with constitutively active E275D Slo2.1 channels. As described in more detail later (see Fig. 7), E275D mutant channels exhibit constitutive activity; i.e., $I_{Slo2.1}$ was detectable in the absence of NFA or elevated $[Na^+]_i$. For these experiments, block of E275D $I_{Slo2.1}$ by 100 µM verapamil was assayed using two different pulse train protocols. For both protocols, the V_h was −120 mV and test pulses were applied to +60 mV. For protocol 1, pulse duration was 3 s and pulses were applied once every 5 s. For protocol 2, pulse duration was 0.3 s and pulses were applied once every 30 s. The relative conductance (G/G_{max}) of E275D Slo2.1 varies from 0.15 at −120 mV to 0.42 at +60 mV. Thus, the relative open probability of channels during protocol 1 would be about twice as long as for protocol 2. For example, with protocol 1, channels are estimated to be open 31% of the time during the first 30 s of the pulse train (6 pulses × [2.0 s × 0.15 + 3.0 s × 0.42] = 9.36 s; 9.36 s/30 s = 0.31). For protocol 2, channels are estimated to be in an open state 15% of the time during the first 30 s (1 pulse × (29.7 s × 0.15 + 0.3 s × 0.42) = 4.58 s; 4.58 s/30 s = 0.15). As shown in Fig. 1 H,

the onset rate for reduction of current was the same for both pulse protocols. These findings indicate that block of E275D Slo2.1 current by verapamil is independent of channel state. A diagram summarizing experiments with verapamil and D890 is shown in Fig. 1 I.

We next determined if the molecular determinants of verapamil block of $I_{Slo2.1}$ were consistent with binding to the central cavity of Slo2.1 channels. Open channel blockers of voltage-gated Ca^{2+} channels (Hockerman et al., 1995, 1997) and Kv channels (Mitcheson et al., 2000; Decher et al., 2004) bind to specific residues that are located in the S6 segment and base of the pore helix that face toward the central cavity. Therefore, we individually mutated residues in Slo2.1 located near the intersection of the pore helix and selectivity filter (Ser 241 and Thr242), and Cys264 to Leu277 in the S6 segment (underlined residues in Fig. 2 A) to determine if mutant channels had an altered sensitivity to verapamil. As discussed under the next heading, three of the S6 mutant channels did not express (P271A, Q273A, and

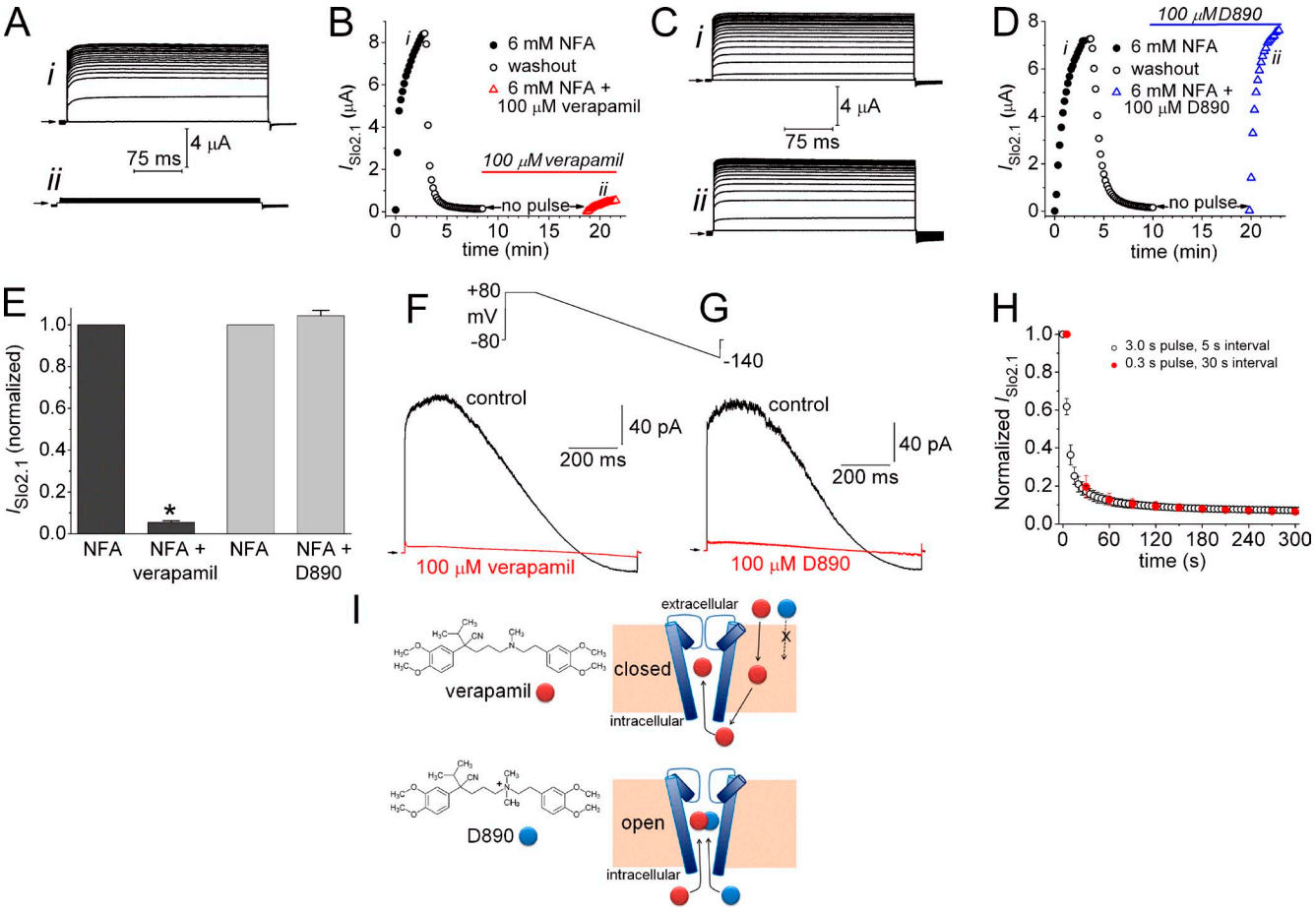

Figure 1. State-independent block of Slo2.1 channels by verapamil and D890. (A) Activation of $I_{Slo2.1}$ during repetitive pulsing to 0 mV (0.3-s duration, 10-s interpulse interval) by 6 mM NFA under control conditions (*i*), and after a 10-min equilibration with 100 μM verapamil (*ii*). (B) Time course of $I_{Slo2.1}$ in a single oocyte during activation with 6 mM NFA, washout of NFA, incubation with 100 μM verapamil for 10 min, and reapplication of 6 mM NFA in the continued presence of verapamil. The oocyte was clamped at −90 mV and pulsed to 0 mV every 10 s except during the 10-min incubation with verapamil. The notations "*i*" and "*ii*" correspond to the currents shown in A. (C and D) External application of 100 μM D890 does not block $I_{Slo2.1}$. Protocol and notations are the same as noted for A and B. (E) Plot of normalized and mean peak $I_{Slo2.1}$ induced by 6 mM NFA alone and by 6 mM NFA in the presence of 100 μM verapamil ($n = 6$; *, $P < 0.0001$) or D890 ($n = 8$) after a 10-min pulse-free equilibration period. Error bars indicate mean ± SEM. (F and G) Mean currents (18–25 consecutive sweeps) recorded from inside-out excised macropatches during voltage ramps from +80 to −140 mV. Currents were recorded in the absence (control) and presence of 100 μM verapamil (F) or 100 μM D890 (G). Arrows indicate 0 current level. (H) Time course of E275D $I_{Slo2.1}$ block by 100 μM verapamil, added to the extracellular solution, measured in response to a train of test pulses applied to +60 mV. Two pulse train protocols are compared. One protocol used 3-s pulses that were applied once every 5 s (open circle, $n = 6$). The other protocol used 0.3 s pulses that were applied once every 30 s (red circle, $n = 6$). Currents were normalized to $I_{Slo2.1}$ measured before drug treatment, and each oocyte was subjected to only one pulse train. Error bars indicate mean ± SEM. (I) Diagram illustrating proposed mechanism of Slo2.1 channel block by verapamil and its quaternary amine derivative D890. Verapamil, but not D890, can cross the cell membrane into the cytoplasm. When applied to the bathing solution of inside/out patches, both compounds can block channels in a state-independent manner, which suggests that the S6 segments do not form a physical barrier to drug entry into the central cavity.

E275A). The effects of verapamil on $I_{Slo2.1}$ recorded from WT and the 13 mutant channels that were expressed were evaluated at 15 µM, a concentration that caused an ∼50% block of current. The point mutations S241T (but not S241A) and F274A (and F274T) reduced channel sensitivity to verapamil, whereas V268A channels were more sensitive to the drug (Fig. 2 B). A homology model of the Slo2.1 channel pore based on the MthK open channel structure predicts that the side chains of Phe274 and Ser241 face toward, whereas Val268 faces away, from the central cavity (Fig. 2 C). The concentration dependence of verapamil block was determined for WT, V268A, and F274T Slo2.1 channels activated by 1 mM NFA (Fig. 2, D and E). The IC_{50} was 14.5 ± 0.6 µM for WT Slo2.1 channels and 4.6 ± 2.3 µM for V268A channels. It is unclear why V268A channels exhibited greater sensitivity to verapamil, but one possibility is that the mutation enhances interaction between the drug and Phe274 residues located two helical turns away in each S6 segment. Unlike WT channels, F274T channels exhibited substantial constitutive activity, allowing us to determine verapamil sensitivity of these mutant channels with or without prior activation by NFA. Verapamil block of constitutively active F274T channels (IC_{50} = 53.0 ± 2.4 µM) was the same as that determined for NFA-activated F274T channels (IC_{50} = 58.7 ± 9.4 µM). These findings suggest that interactions with one or more Phe274 and Ser241 residues, which modeling suggests face toward the inner pore, are important molecular determinants of verapamil block of Slo2.1 channels.

In summary, D890 blocked Slo2.1 only when applied to the cytoplasmic side of the membrane, and verapamil produced nearly complete block when applied to non-activated (closed) WT channels and blocked E275D channels independent of channel open time. Verapamil interacts with residues that are predicted to face toward the central cavity of the Slo2.1 channel. Together, these findings indicate that the S6 bundle crossing does not restrict access of large phenylalkylamines to the inner pore of nonconducting Slo2.1 channels.

Ala scanning mutagenesis of the S6 segment identifies key residues involved in Slo2.1 channel activation

Our findings suggest that similar to Slo1 channels (Chen and Aldrich, 2011; Thompson and Begenisich, 2012), the S6 bundle crossing does not serve as the primary barrier

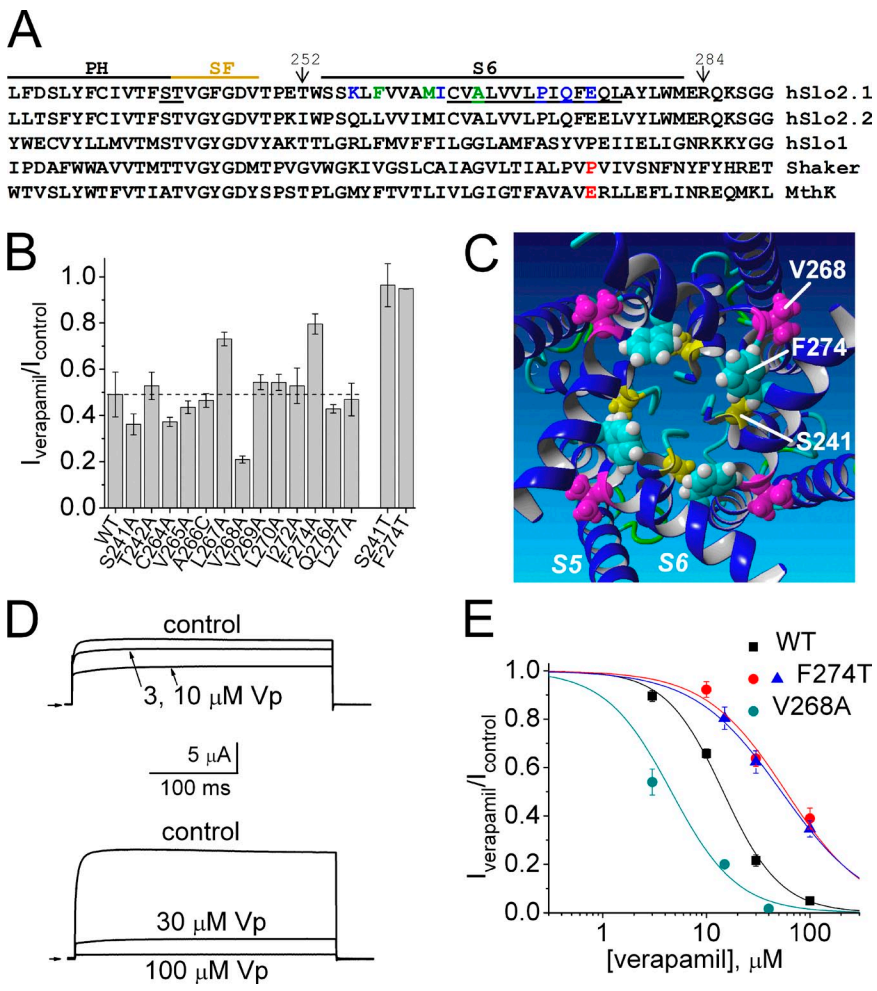

Figure 2. Molecular determinants for verapamil block of Slo2.1 channels. (A) Amino acid sequence alignment of the pore region of Slo2.1 with other K^+ channels. Sequence alignment begins with pore helix (PH) followed by the selectivity filter (SF) and S6 segment. Ser241, Thr242, and residues in S6 of human Slo2.1 that were mutated to Ala are underlined. Mutation of colored residues to Ala caused gain of function (green) or loss of function (blue). P475 in Shaker and E92 in MthK channel are colored red. (B) Bar graph summarizing relative block of $I_{Slo2.1}$ ($I_{verapamil}/I_{control}$) by 15 µM verapamil for WT channels and channels with indicated point mutation. The broken horizontal line indicates $I_{verapamil}/I_{control}$ value for WT channels. Currents were activated by 1 mM NFA and elicited with 300-ms pulses to 0 mV. Error bars indicate mean ± SEM. (C) Homology model of Slo2.1 pore domain viewed from cytoplasmic side and showing side chains of Ser241 (yellow), Val268 (magenta), and Phe274 (cyan). (D) Concentration-dependent block of WT Slo2.1 channel currents by verapamil. $I_{Slo2.1}$ activated by 1 mM NFA in the absence (control) and presence of indicated [verapamil]. Pulses were applied to 0 mV for 300 ms. (E) [Verapamil]–response curve for WT and mutant Slo2.1 channels. The IC_{50} was 14.5 ± 0.6 µM (n_H = 1.5 ± 0.1; n = 7) for WT channels, 58.7 ± 9.4 µM (n_H = 1.1 ± 0.2, n = 6) for F274T channels activated by 1 mM NFA (red circles), 53.0 ± 2.4 µM (n_H = 1.0 ± 0.06, n = 4) for constitutively active F274T channels (blue triangles), and 4.6 ± 2.3 µM (n_H = 1.4 ± 0.5, n = 4) for V268A channels (teal circles). Error bars indicate mean ± SEM.

to ion permeation (i.e., an activation gate) for Slo2.1 channels. While apparently not forming a barrier to ion permeation, the S6 segments of Slo1 undergo dynamic rearrangement during channel opening and closing (Chen and Aldrich, 2011) to allosterically couple the binding of intracellular Ca^{2+} (to the C-terminal domain) to the selectivity filter. According to this model, the selectivity filter functions as the primary activation gate. To investigate whether the S6 might also be intimately involved in the gating of Slo2.1, Ala scanning mutagenesis of the S6 segment, from Thr252 to Arg284 (Fig. 2 A), was performed to identify residues crucial for normal channel function. The three native Ala residues located in this region of S6 were mutated to Cys. Oocytes were injected with 0.2–2 ng cRNA and recorded 1–3 d later to achieve comparable levels of expression for all mutant channels. The peak magnitudes of $I_{Slo2.1}$ activated by a pulse to 0 mV in the presence of 1 and 6 mM NFA are summarized in Fig. 3 A for each mutant channel. When mutated to Ala, five residues in S6 (Lys256, Ile263, Pro271, Gln273, and Glu275) caused loss of channel function; i.e., currents induced by 6 mM NFA in mutant cRNA-injected oocytes were not discernible from currents recorded from uninjected oocytes. However, very weak functional expression of K256A, I263A, and Q273A Slo2.1 channels was achieved 3–4 d after oocytes were injected with large amounts (10 ng) of cRNA and activated with NFA (Fig. 3 B). Slo2.1 channels can also be activated by loading of cells with NaCl by diffusion from standard (not agarose tipped) recording pipettes filled with 2.4 M NaCl. Activation of $I_{Slo2.1}$ by intracellular NaCl loading in a single oocyte is shown in Fig. 4 A. A comparison of current magnitude induced by intracellular NaCl loading as a function of time for uninjected oocytes and those expressing WT Slo2.1 channels is shown in Fig. 4 B. Oocytes injected with cRNA for K256A, I263A, and Q273A Slo2.1 channels were also activated by intracellular NaCl loading, but the mutant channel currents were ~5–15-fold smaller than WT channel currents (Fig. 4 C). Neither NFA (Fig. 3 B) nor NaCl loading (Fig. 4 D) were able to activate currents in oocytes injected with 10 ng of cRNA encoding P271A (or P271G, not depicted) or E275A Slo2.1 channels.

The cell surface expression of poorly expressing and nonfunctional S6 mutant channels was assayed by Western blotting (Fig. 5). To certify the relative purity of the biotinylated membrane preparation, gels loaded with this membrane fraction (Fig. 5 A) or the cytoplasmic fraction (Fig. 5 B) were probed with antibodies directed toward Na^+/K^+ ATPase (a plasma membrane marker) and GAPDH (a cytoplasmic marker). The strong labeling of ATPase in the membrane fraction, but not in the cytoplasmic fraction, and the opposite pattern for GAPDH indicates that the plasma membrane fraction was adequately isolated. Based on densitometry analysis, oocytes injected with 10 ng WT Slo2.1 cRNA resulted in a surface protein expression that was 1.5-fold greater than for oocytes injected with 1 ng cRNA (Fig. 5 A, top), which indicates that 3 d after injection, 1 ng cRNA was sufficient to nearly saturate expression/trafficking of Slo2.1 channels to the cell membrane. The surface expression of K256A, I263A, Q273A, and E275A channel proteins were noticeably reduced compared with WT channels (Fig. 5 A, top). The relative surface expression of mutant Slo2.1 proteins (normalized to Na^+ pump protein) was estimated by comparison to WT Slo2.1 (10 ng cRNA) in Fig. 5 C. Surface expression of K256A, Q273A, and E275A mutant proteins was approximately fivefold less than WT protein. I263A protein expression was reduced ~20-fold. The P271A protein expression level was equivalent to WT protein, despite the total absence of measurable current in oocytes. Fig. 5 C also compares the magnitude of mutant channel currents

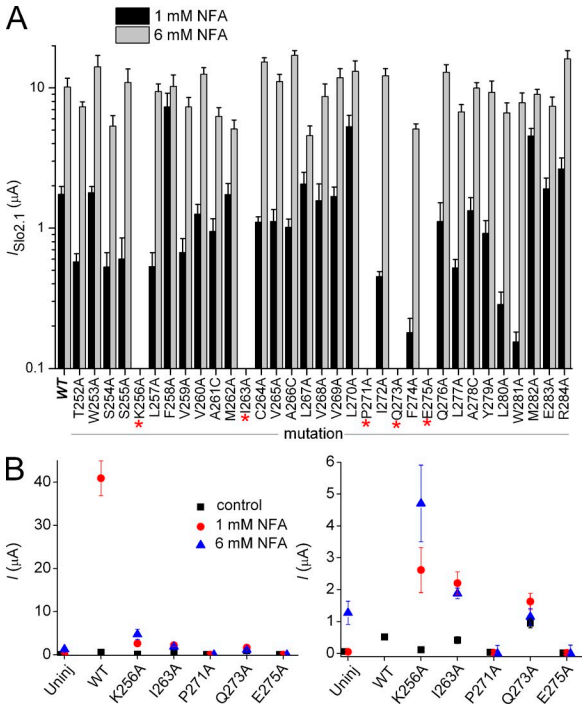

Figure 3. Mutagenesis scan of S6 segment identifies residues important for normal Slo2.1 channel gating. (A) 33 consecutive residues (Thr252 to Arg284) located in the S6 segment were individually mutated to Ala (native Ala residues were mutated to Cys), and the effect of 1 and 6 mM NFA on $I_{Slo2.1}$ was quantified at a test potential of 0 mV. Oocytes were injected with 0.2–2 ng cRNA and recorded 1–3 d later ($n = 4$–6). Five mutations (K256A, I263A, P271A, Q273A, and E275A) caused complete loss of channel function (indicated by the asterisks). (B) Plot of peak currents measured at 0 mV in the absence (black boxes) and presence of 1 mM NFA (red circles) and 6 mM NFA (blue triangles) for the five loss-of-function mutant channels. Mutant channel currents measured in presence of 6 mM NFA were corrected by subtraction of the mean value for endogenous currents activated by 6 NFA in uninjected oocytes. Oocytes were injected with 10 ng of cRNA and incubated for 3–4 d ($n = 6$–10). The right panel shows the same data plotted on an expanded y axis. Error bars indicate mean ± SEM.

activated by either NFA or internal NaCl loading, normalized to WT currents. This analysis revealed that the reduction in current magnitude of K256A, I263A, and Q273A mutant channels can be largely accounted for by the reduction in surface protein, presumably a consequence of protein misfolding. In contrast, the complete loss of function (absence of currents) observed for E275A mutant channels can only partially be explained by a disruption in protein trafficking. Together these findings suggest that P271A and E275A mutations prevent channel opening.

Glu275 prevents formation of the S6 bundle crossing

Based on sequence alignment (Fig. 2 A), Glu275 is in a position homologous to key S6 residues of Kv channels that when mutated to an acidic residue (e.g., P475D in Shaker B channels; Hackos et al., 2002) induce voltage-independent, constitutive channel opening. Conversely, neutralization of the acidic residue Glu92 in the equivalent position of the inner helix of MthK bacterial channels induces channel closure (Parfenova et al., 2006). By analogy, Glu275 might prevent formation of a tight S6 bundle crossing in Slo2.1 channels. To test this idea, Glu275 was substituted with several other amino acids to determine if there was a correlation between physicochemical features (charge, hydrophobicity, etc.) of the introduced residue and the ability of the resulting mutant channel to be activated by NFA. To maximize responses, currents activated in response to 1 and 6 mM NFA were recorded from oocytes 2 d after injection with 10 ng *Slo2.1* cRNA. Mutation of Glu275 to other hydrophobic residues (Gly, Val, Phe, Trp) or polar residues (Ser, Cys) caused complete loss of function. Channel function was retained when Glu275 was mutated to highly polar (Gln, Asn) or basic (Arg, Lys) residues, although currents were reduced in magnitude or required higher concentrations of NFA for activation. E275H channel currents were very small and not clearly discernible from background currents. These findings are summarized in Fig. 6 where current magnitudes at 0 mV are plotted as a function of hydrophobicity for the amino acids substituted for Glu275. For this plot, the GES (Goldman, Engelman, Steitz) hydrophobicity scale was used as it is based on energetic considerations of residues in an α-helix derived from experimental data (Engelman et al., 1986). Functional channel activity was measurable only when Glu275 was substituted with a residue with a ΔΔG value for water-membrane free energy transfer <−3 kcal/mol.

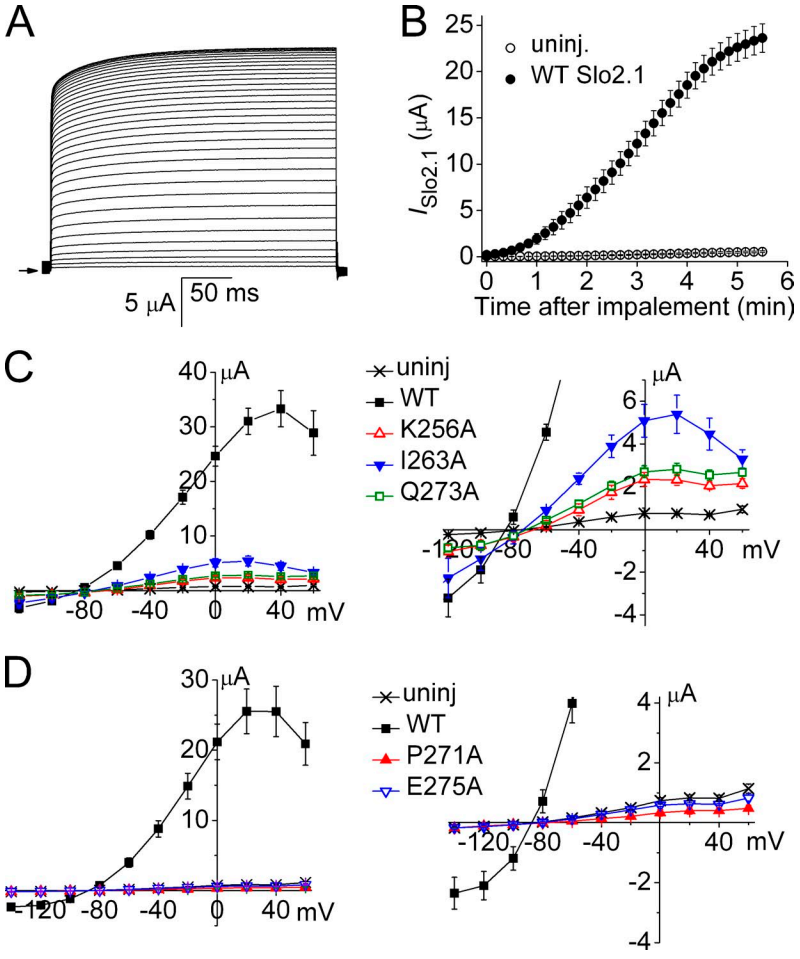

Figure 4. Intracellular NaCl loading of oocytes activates a robust $I_{Slo2.1}$ in oocytes expressing WT Slo2.1, but not in oocytes expressing S6 mutant channels that did not respond to NFA treatment. (A) Time course of $I_{Slo2.1}$ activation induced by leakage of NaCl from recording pipettes in a single oocyte injected with 10 ng WT Slo2.1 cRNA. Currents were elicited with 300-ms pulses applied to 0 mV every 10 s for a total of 5 min, 40 s. The first current (smallest amplitude) was recorded immediately after impalement of the oocyte. The arrow on left indicates 0 current level. (B) Mean time course of $I_{Slo2.1}$ activation induced by intracellular NaCl loading for cells recorded 3 d after injection with 10 ng WT Slo2.1 cRNA (n = 12) compared with uninjected cells (n = 12) from the same batch of oocytes. Currents were measured at the end of 300-ms pulses applied to 0 mV every 10 s. (C) NaCl loading activates small currents in oocytes expressing K256A, I263A, and Q273A mutant channels. The right panel shows data with an expanded y axis. (D) P271A and E275A mutant channels are not activated by NaCl loading. The right panel shows data with an expanded y axis. Error bars indicate mean ± SEM.

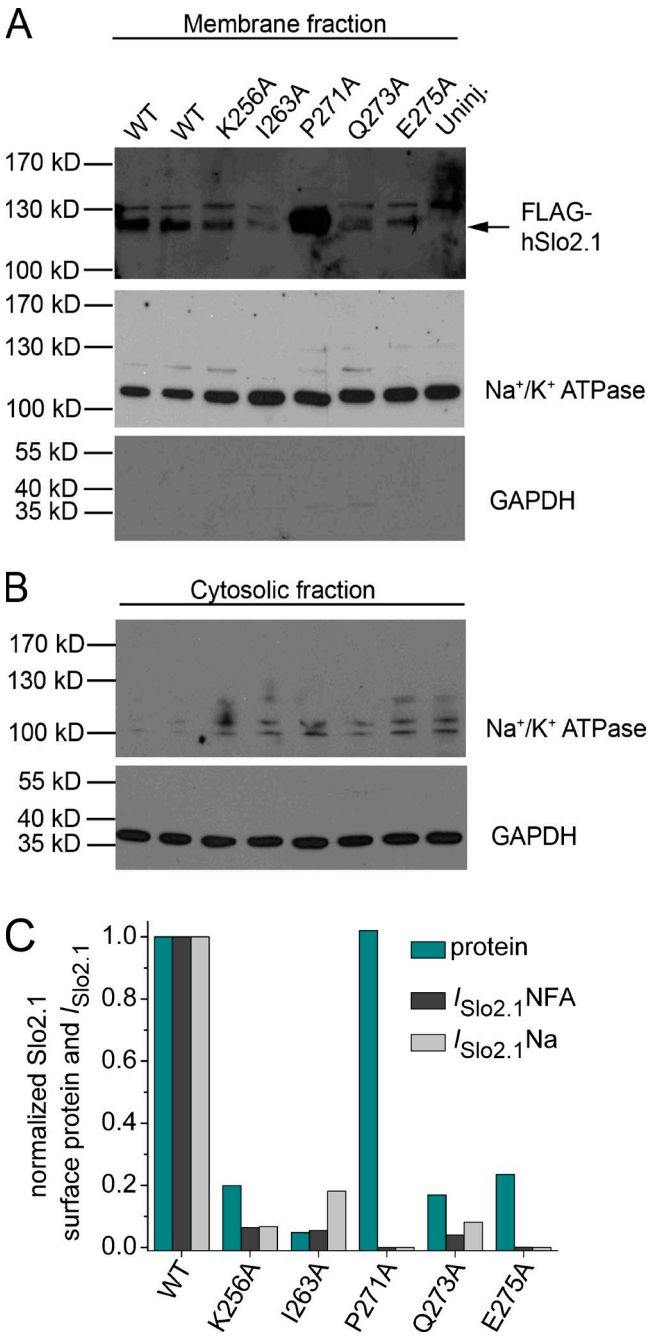

Figure 5. Western blot analysis of oocytes expressing WT and S6 mutant Slo2.1 channels. (A) Proteins in the biotinylated membrane fraction were separated by SDS-PAGE electrophoresis, and gels were blotted to detect FLAG-tagged Slo2.1. In the top panel, Slo2.1 monomer is represented by a 120-kD band, which is absent in uninjected oocytes. The 130-kD band in the top panel was detected in all lanes and represents nonspecific labeling by the antibody. For the top panel, lanes 1 and 2 were loaded with samples from oocytes injected with 10 and 1 ng WT FLAG-tagged *Slo2.1* cRNA, respectively. For all other panels, lanes 1 and 2 represent samples from oocytes injected with 1 and 10 ng WT FLAG-tagged *Slo2.1* cRNA, respectively. Na^+/K^+ ATPase (plasma membrane marker), but not GAPDH (cytosolic marker), was present in this fraction. (B) Western blots for Na^+/K^+ ATPase and GAPDH from the cytosolic fraction. (C) Comparison of relative surface protein expression and current magnitude for WT and S6 mutant Slo2.1 channels. Western blots in A were quantified by densitometry using the area under the curve method of ImageJ software to correct for background noise, and the nonspecific 130-kD band observed in all lanes, including the uninjected oocytes lane. The ratio of FLAG-tagged Slo2.1 Na^+/K^+ ATPase band intensities from the same membrane fraction sample was determined for each lane. The relative band intensity of mutant Slo2.1 proteins (cyan bars) were calculated by normalization to the ratio determined for the sample of oocytes injected with 10 ng WT cRNA. Currents were measured at 0 mV after activation with either 1 mM NFA ($I_{Slo2.1}$NFA, calculated from data plotted in Fig. 3 B) or by intracellular loading with NaCl ($I_{Slo2.1}$Na, calculated from data plotted in Fig. 4, C and D).

In other words, opening of Slo2.1 channels only occurred if residue 275 in the S6 segment was a highly polar or charged residue.

The most highly conserved mutation of Glu275, E275D, induced a gain of function. Large currents were observed in oocytes injected with 1 ng E275D cRNA in the absence of ligand-mediated activation (Fig. 7, A and B). This finding is in contrast to WT channels, where $I_{Slo2.1}$ was not detectable in oocytes injected with the same amount of cRNA unless activated by NFA. The properties of E275D channel currents in the absence of NFA were similar in many ways to WT channel currents activated by 1 mM NFA (Dai et al., 2010). First, similar to WT Slo2.1 (Dai et al., 2010), the magnitude of outward E275D $I_{Slo2.1}$ was decreased when $[K^+]_e$ was elevated from 2 to 104 mM by more than that could be accounted for by the shift in E_K, the equilibrium potential for K^+ (Fig. 7 B). Second, the weak voltage dependence of constitutive E275D channel activation (Fig. 7 C: $V_{0.5}$ = 92.4 mV; z = 0.48 *e*) was the same as WT Slo2.1 channels partially activated with 1 mM NFA (Dai et al., 2010). Third, in response to membrane depolarization, E275D $I_{Slo2.1}$ was composed of instantaneous and time-dependent components. Over the voltage range from −20 to +80 mV, the relative amplitude of the instantaneous component was decreased from 0.77 to 0.55, whereas conversely the amplitude of the biphasic, time-dependent component of current were increased (Fig. 7 D). The time constant (τ) for the fast component of time-dependent current was ∼25 ms, 4–5 times faster than τ for the slow component that ranged from 105 ms at −20 mV to 130 ms at +80 mV (Fig. 7 E). E275D Slo2.1 channels were not fully open and currents could be enhanced by NFA. The [NFA]–response relationship (Fig. 7 F) indicates that the constitutive activity of E275D channels (current in the absence of NFA) was equivalent to ∼40% of the maximum activity achieved with NFA. By comparison, the constitutive activity of WT Slo2.1 channels in nonactivated oocytes was estimated to be ∼0.5% of maximum (Dai et al., 2010). Moreover, E275D channels were more sensitive to NFA compared with WT channels. The EC_{50} for NFA activation of E275D channels was 192 µM, 11-fold

lower than the EC_{50} (2.1 mM) for WT channels (Dai et al., 2010; Garg and Sanguinetti, 2012). The effects of a maximally effective concentration of NFA (3 mM) on the kinetics and magnitude of E275D channels (Fig. 7, G–I) were nearly the same as that achieved by loading oocytes with NaCl via the pipette solution (Fig. 7, J–L). The maximal increase in current at 0 mV (~2.5-fold) was the same, and currents became instantaneous at all test potentials, which suggests that both interventions resulted in maximal channel activation. Constitutively active E275D channels should prove useful for characterizing the biophysical properties of Slo2.1 channels in the absence of an activating ligand.

The finding that channel opening requires the presence of Glu or another very hydrophilic amino acid at position 275 in S6 suggests that the side chain of this residue faces toward the water-filled central cavity. Glu275 residues could prevent formation of a bundle crossing, either by intersubunit electrostatic repulsion or by maintaining the S6 segments in a configuration incompatible with formation of a tight bundle crossing. Evidently, when Glu275 is substituted with a hydrophobic residue, the mutant channel assumes a permanently closed state that resists activation by extracellular NFA or elevated $[NaCl]_i$. To determine whether Glu275 is uniquely positioned to prevent formation of a tight bundle crossing, we determined if the function of E275A channels could be recovered by introducing a Glu residue into a different, nearby position of the S6 α-helix.

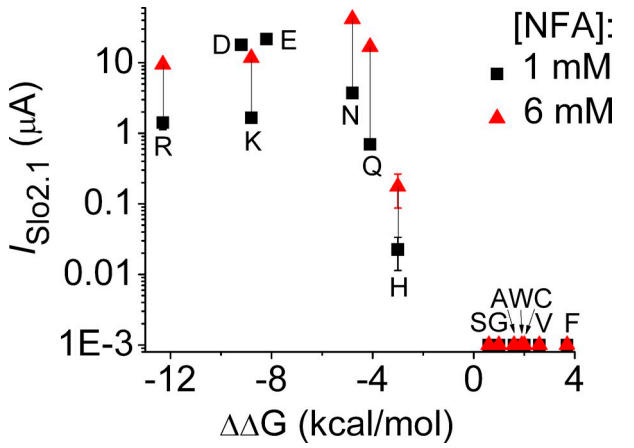

Figure 6. Slo2.1 channels with hydrophobic substitutions of Glu275 are nonfunctional. The peak magnitude of currents recorded at the end of 0.3-s pulses to 0 mV in response to 1 and 6 mM NFA are plotted as a function of the GES hydrophobicity scale value for free energy transfer from water to membrane (Engelman et al., 1986) for the indicated Glu275 substitution (in single letter code). WT channels are indicated as "E." $I_{Slo2.1}$ for E275D channels ("D") represents constitutive activity (no NFA) in oocytes injected with 1 ng cRNA and recorded after 3 d ($n = 5$). Currents in WT channels and for all other mutant channels were measured in oocytes 2 d after injection with 10 ng of *Slo2.1* cRNA (for WT channels, $n = 10$; for mutant channels, $n = 5$). Error bars indicate mean ± SEM.

As shown in Fig. 8 (A–C), rescue of E275A channels was achieved by mutation of Ala278 to Glu (or Arg) or Tyr279 to Glu. However, substitution of Gln276, Leu277, or Leu280 did not rescue channel function (Fig. 8, D–F). A helical wheel plot of S6 residues predicts that Ala278 and Tyr279 are located near the same half of the α-helix as Glu275, whereas Gln276, Leu277, or Leu280 are located on the opposite half (Fig. 8 G). The MthK-based homology model of the Slo2.1 pore domain predicts that Glu275, Ala278, and Tyr279 face the central cavity (Fig. 8 H), whereas Gln276, Leu277, and Leu280 do not (Fig. 8 I). We conclude that appropriately positioned Glu residues in S6 prevent the S6 segments from forming a tight bundle crossing and that, therefore, another region of the channel must be responsible for gating K^+ ion permeation. We next explored the possibility that the selectivity filter acts as the primary barrier to ion permeation (i.e., serves as the activation gate) in Slo2.1 channels.

Intrasubunit coupling between S5, S6, and the pore helix alters activation state of Slo2.1

The homology model of the Slo2.1 pore domain was used to predict potential intrasubunit interactions between the S6 segment and the pore helix (Fig. 9 A). The model predicts interaction between four residues in the pore helix (Phe235, Cys236, Thr239, and Phe240) and four residues in S6 (Val259, Met262, Ile263, and Ala266). We first considered the S6 residues. As summarized in Figs. 3 and 9 B, substitution of Val259 with Ala had no obvious functional effects, whereas I263A channels exhibited increased sensitivity to NFA and loss of function that can be attributed to a decrease in trafficking of mutant protein to the cell surface (Fig. 5). To determine if mutation of Met262 and Ala266 also increased sensitivity to NFA, concentration–response relationships were determined for M262A and A266G. A266C channels were already determined to have no functional effect (Fig. 3 A); therefore, A266G was chosen for analysis because Gly has a smaller side chain volume and can also produce a bend in the α-helical structure. Although the model does not predict that Phe258 interacts with the pore helix, we also included F258A channels for further analysis because this mutant channel appeared to be more sensitive to NFA (Fig. 3 A). All three mutations (F258A, M262A, and A266G) induced a gain of channel function, defined as constitutive activity in the absence of NFA and enhanced sensitivity to NFA (Fig. 9, B–E) as indicated by leftward shifts in the [NFA]–response relationships (Fig. 9 F). The relative magnitude of constitutive current for mutant channels ($I_{c\text{-}rel}$) was defined as peak $I_{Slo2.1}$ (at 0 mV) in the absence of NFA divided by $I_{Slo2.1}$ after maximal activation by NFA. $I_{c\text{-}rel}$ was 0.34 for F258A, 0.12 for A266G, and 0.04 for M262A channels (Fig. 9 F). All three mutations reduce side chain volumes compared

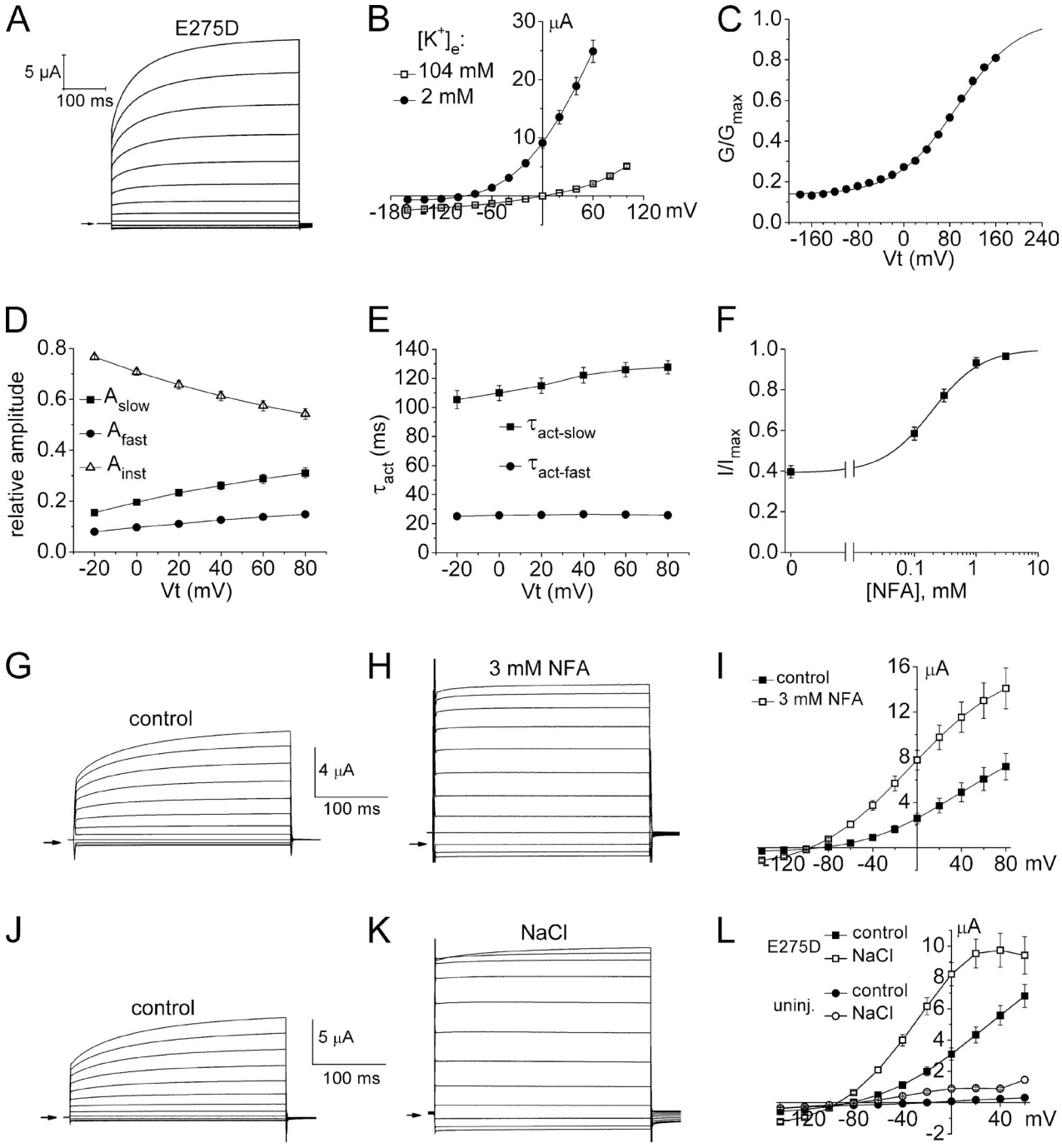

Figure 7. A highly conserved mutation in S6, E275D, enhances channel opening probability. (A) Currents recorded from an oocyte expressing E275D Slo2.1 channels without NFA treatment. (B) *I*-V_t relationship for E275D Slo2.1 channels with $[K^+]_e$ of 2 and 104 mM (1 ng cRNA/oocyte; 2 d expression; $n = 8$). (C) G-V relationship for E275D channels calculated from $I_{Slo2.1}$ recorded from oocytes bathed in K104 solution ($n = 4$). Data were fitted with a Boltzmann function (smooth curve) to estimate $V_{0.5}$ (92.4 ± 1.4 mV), z (0.48 ± 0.01 *e*), and minimum G/G_{max} (0.14). (D) Relative amplitudes of instantaneous (A_{inst}), and the fast (A_{fast}) and slow (A_{slow}) time-dependent components of E275D $I_{Slo2.1}$. (E) Time constants for activation of E275D $I_{Slo2.1}$. For D and E, oocytes were injected with 1 ng cRNA and recorded 2 d later ($n = 11$). (F) [NFA]–response relationship for E275D Slo2.1 channels. Data were fitted with a logistic equation (smooth curve) to calculate EC_{50} (192 ± 25 μM) and n_H (1.08 ± 0.09, $n = 10$). (G and H) E275D $I_{Slo2.1}$ recorded in the same oocyte under control conditions (G) and after further activation by 3 mM NFA (H). V_h was −90 mV and pulses were applied in 20-mV steps to a V_t that ranged from +80 to −140 mV. (I) Mean *I*-V_t relationships for oocytes expressing E275D Slo2.1 channels (1 d after injection with 0.5 ng cRNA) under control conditions and after treatment with 3 mM NFA ($n = 5$). (J and K) E275D $I_{Slo2.1}$ recorded in the same oocyte under control conditions (J) and after further activation by intracellular loading with NaCl (K). V_h was −90 mV and pulses were applied in 20-mV steps to a V_t that ranged from +80 to −140 mV. (L) Mean *I*-V_t relationships for oocytes expressing E275D Slo2.1 channels ($n = 11$) under control conditions (1 d after injection with 0.4 ng cRNA) and after NaCl loading (NaCl), and uninjected oocytes ($n = 5$) before (control) and after NaCl loading (NaCl). Error bars indicate mean ± SEM.

with the native S6 residue and, thus, would be expected to reduce the overall intrasubunit interaction between S6 and the pore helix. However, as the functional impact of these mutations on channel gating are rather modest, it is not clear if any of these three residues are directly involved in gating of Slo2.1 channels.

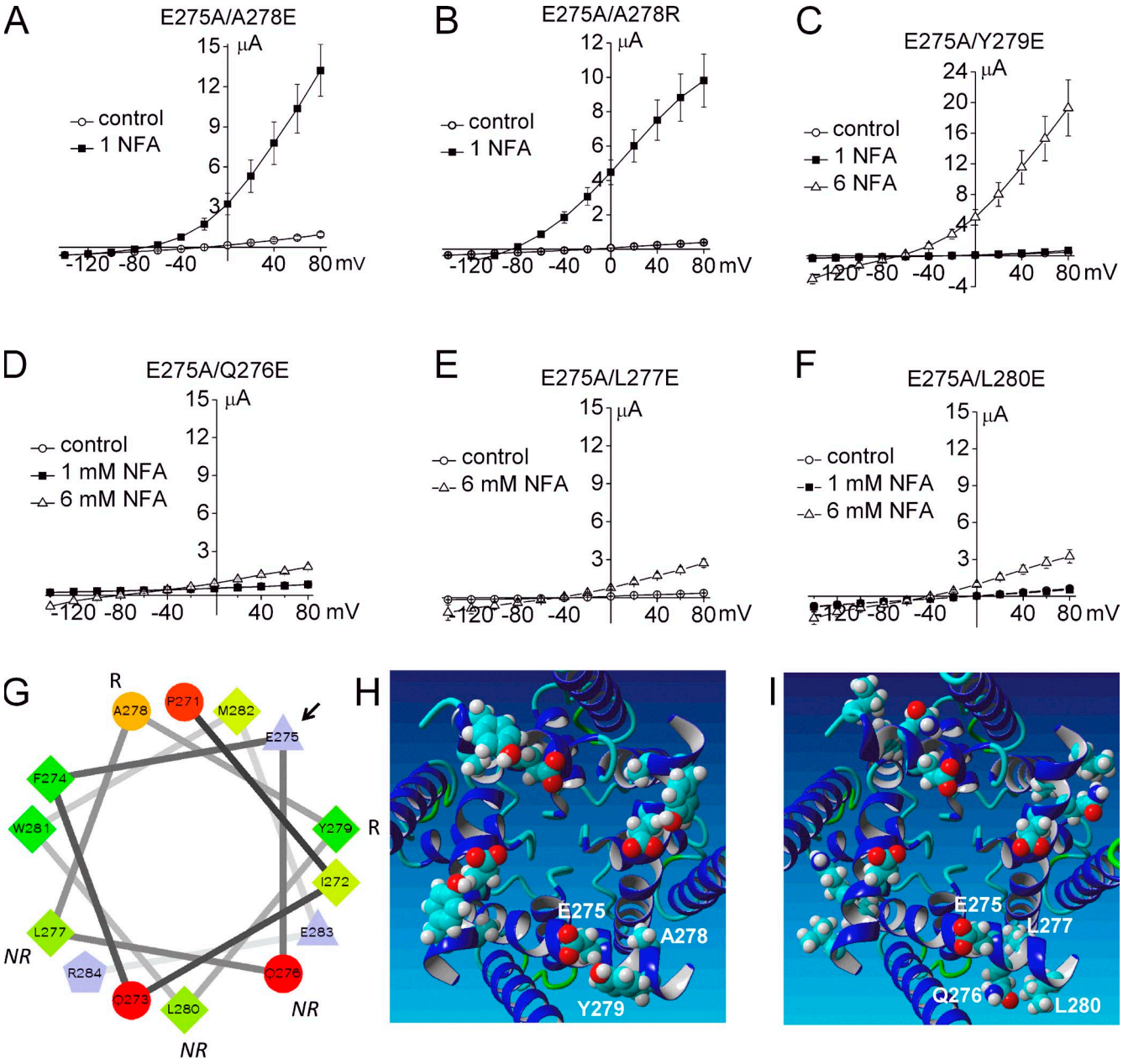

Figure 8. Intragenic rescue of nonfunctional E275A Slo2.1 was achieved by introducing a charged residue one helical turn away in the S6 segment. Mean I-V_t relationships recorded before (control) and after treatment of oocytes with NFA for E275A/A278E channels (A; $n = 5$; 5 ng cRNA injected, currents recorded after 4 d), E275A/A278R channels (B; $n = 8$; 1 ng cRNA injected, currents recorded after 2 d), and E275A/Y279E channels (C; $n = 6$; 10 ng cRNA injected, currents recorded after 4 d). (D–F) E275A/Q276E channels (D), E275A/L277E channels (E), and E275A/L280E channels (F). For D–F: $n = 6$; 10 ng cRNA injected, currents recorded after 5 d. Error bars indicate mean ± SEM. (G) Helical wheel plot of S6 segment of Slo2.1 from Pro271 to Arg284. The arrow points to Glu275, R indicates the two residues that when mutated to Glu rescued E275A channel function, and NR indicates the three residues that when mutated to Glu did not rescue E275A channel function. A wheel plot was made using the Wheel.pl program written by D. Armstrong and R. Zidovetzki (http://rzlab.ucr.edu/scripts/wheel/wheel.cgi). Residues are shape- and color-coded to indicate physical properties as follows: circles, uncharged hydrophilic (proportional to the intensity of red color); diamonds, hydrophobic (proportional to the intensity of green color); triangles, acidic; pentagon, basic. (H and I) MthK-based model of the Slo2.1 pore domain (S5-PH-S6) viewed from the intracellular side. Key residues are labeled for one subunit in each panel. Mutation of Ala278 or Tyr279 (H) to Glu rescued function of E275A channels. Mutation of Gln276, Leu277, or Leu280 (I) did not rescue E275A channels.

We next mutated to Ala the four pore helix residues (Phe235, Cys236, Thr239, Phe240) predicted to interact with S6 within the same subunit (Fig. 9 A). F235A channels were nonfunctional (Fig. 9 B), perhaps because this mutation disrupted the network of interacting aromatic residues as described previously for KcsA K^+ channels (Doyle et al., 1998). C236A channels exhibited a partial loss of function (insensitive to 1 mM NFA), and T239A channels responded to NFA similar to WT channels (Fig. 9 B). Mutation of Phe240, located at the base of the pore helix, yielded the most interesting functional effect. F240A channels exhibited considerable constitutive activity ($I_{c\text{-}rel}$ = 0.35) and were more sensitive to NFA (Fig. 9 B). The role of Phe240 in channel gating was further investigated by additional mutations of this residue. Mutations induced a variable amount of constitutive channel activity (Fig. 10 A). The most conserved mutation, F240Y, had no functional effect on channel gating, whereas with the exception of Trp, $I_{c\text{-}rel}$ increased as a function of hydrophilicity of the residue substituted for Phe240 (Fig. 10 B). Mutation of Phe240 to polar residues Cys or Thr decreased channel expression, but caused the most dramatic increase in constitutive channel activity. The $I_{c\text{-}rel}$ of F240C and F240T mutant channels was 1.0; i.e., currents were time independent and not further activated by NFA. Two other polar residue substitutions (F240N and F240S) yielded channels that expressed very poorly, were less K^+-selective (E_{rev} = −20 mV), and were not activated by NFA. Because expression was so poor, these two mutant channels were not further characterized. Further evidence that the F240C channels were maximally activated was the finding that neither external application of 1 mM NFA (Fig. 10 C) nor intracellular loading of NaCl (Fig. 10 D) caused any further increase in $I_{Slo2.1}$ over a wide voltage range, from −140 to +60 mV. In contrast, when $[K^+]_e$ was elevated to 104 mM, F240C channels were further activated by 1 mM NFA (Fig. 10 C). We previously reported the same $[K^+]_e$-dependence of channel activity for constitutively active R190E Slo2.1 channels (Dai et al., 2010). Thus, Phe240 is a key structural determinant of Slo2.1 channel gating.

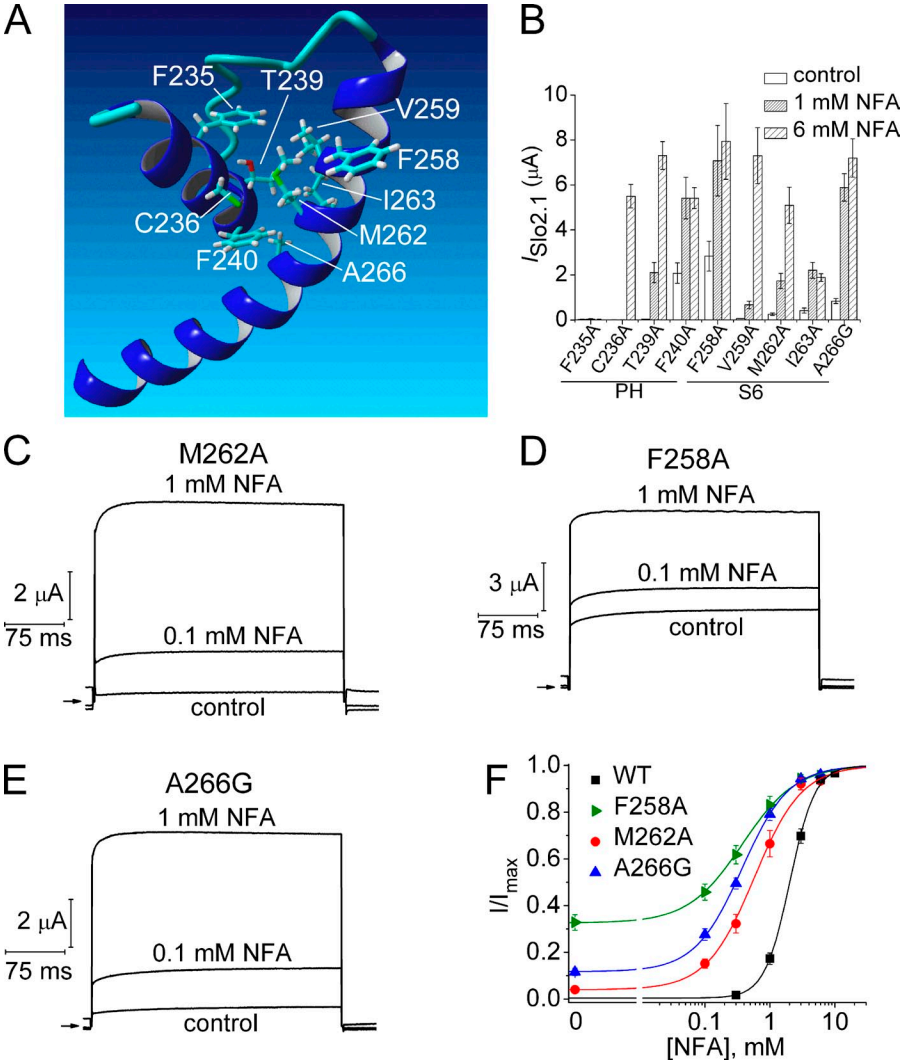

Figure 9. Point mutation of S6 residues that face the pore helix exhibit enhanced sensitivity to NFA. (A) Homology model of pore helix and S6 segment of one Slo2.1 subunit highlighting potential residue interactions. (B) Peak outward currents measured at 0 mV in the absence (control) and presence of 1 and 6 mM NFA for channels with point mutations of the native residues in the pore helix (PH) or S6 highlighted in A (n = 5–7). (C–E) $I_{Slo2.1}$ recorded from oocytes expressing M262A, F258A, and A266G Slo2.1 channels before (control) and after treatment with 0.1 and 1 mM NFA. Arrows indicate 0 current level. (F) [NFA]–response relationships for WT and gain-of-function S6 mutant channels. Data were fitted with a logistic equation (smooth curve). For WT (n = 9), EC_{50} = 2.1 ± 0.1 mM, n_H = 2.4 ± 0.06; for F258A (n = 7): EC_{50} = 0.4 ± 0.05 mM, n_H = 1.2 ± 0.08; for M262A (n = 6), EC_{50} = 0.66 ± 0.13 mM, n_H = 1.4 ± 0.06; for A266G (n = 5), EC_{50} = 0.38 ± 0.03 mM, n_H = 1.2 ± 0.03. Error bars indicate mean ± SEM.

In addition to the potential interactions between the pore helix and S6 segment highlighted in Fig. 9 A, the Slo2.1 homology model also predicts potential interaction between Phe240 and three residues in the S5 segment (Fig. 11 A). In the model, specific atoms of Leu209, Ile210, and Cys213 are located within <4 Å of the Phe240 side chain. The S5 residues were mutated to Ala and their response to 1 and 6 mM NFA was evaluated. I210A and C213A Slo2.1 channels were similar to WT channels, exhibiting no constitutive activity and an [NFA]-dependent increase in current at 0 mV (Fig. 11 B). L209A channels exhibited constitutive activity ($I_{c\text{-}rel}$ = 0.26) and were more sensitive to NFA (Fig. 11 B). We hypothesized that if a hydrophobic interaction between Leu209 and Phe240 stabilizes the closed state of the channel, then mutating Leu209 to a polar residue would increase open probability, similar to the effect of mutating Phe240 to more polar residues. Indeed, L209T Slo2.1 channels had more constitutive activity than L209A channels. The $I_{c\text{-}rel}$ for L209T was 0.61, threefold greater than L209A, and the EC_{50} for NFA was 106 µM (Fig. 11 C), 20-fold more NFA sensitive than WT Slo2.1. Similar to F240C (Fig. 10 C), elevation of $[K^+]_e$ from 2 to 104 mM caused a parallel shift in the I–V_t relationship for L209T channels. Thus, unlike WT (Dai et al., 2010) and E275D (Fig. 7 E) Slo2.1 channels, the conductance of L209T channels was not reduced by elevated $[K^+]_e$. Finally, the increase in $I_{Slo2.1}$ of L209T channels induced by 1 mM NFA (Fig. 11 E), a maximally effective concentration, matched the increase in $I_{Slo2.1}$ induced by loading cells with NaCl (Fig. 11 F).

Together the findings presented in Figs. 9–11 suggest, albeit somewhat indirectly, that the S6 segment and specific residues in the S5 (Phe240) and the pore helices (Leu209) form an interacting network that modulates the open probability of Slo2.1 channels. Close proximity to these key residues to the selectivity filter implicates it as the most likely structural element that serves as the primary activation gate.

Intragenic rescue of P271A and E275A Slo2.1 channels

Mutation of Pro271 or Glu275 in the S6 segment can cause complete loss of channel function. We attempted to rescue the function of P271A and E275A channels by introducing a second site mutation that by itself can induce a significant gain of function. Four second-site mutations were analyzed, including R190E (Dai et al., 2010) and A278R (Garg and Sanguinetti, 2012), described previously, and F240C and E275D. The charge-reversing mutation R190E located in the S4/S5 linker near the end of the S4 segment of Slo2.1 induces constitutive channel activity that is not further enhanced by NFA (i.e., $I_{c\text{-}rel}$ = 1; Dai et al., 2010), whereas the S6 mutations E275D and A278R (Garg and Sanguinetti, 2012) induce submaximal increases in $I_{c\text{-}rel}$ and are more sensitive to further activation by NFA as compared with WT channels.

We first determined if any of the four gain-of-function mutations could rescue the function of P271A

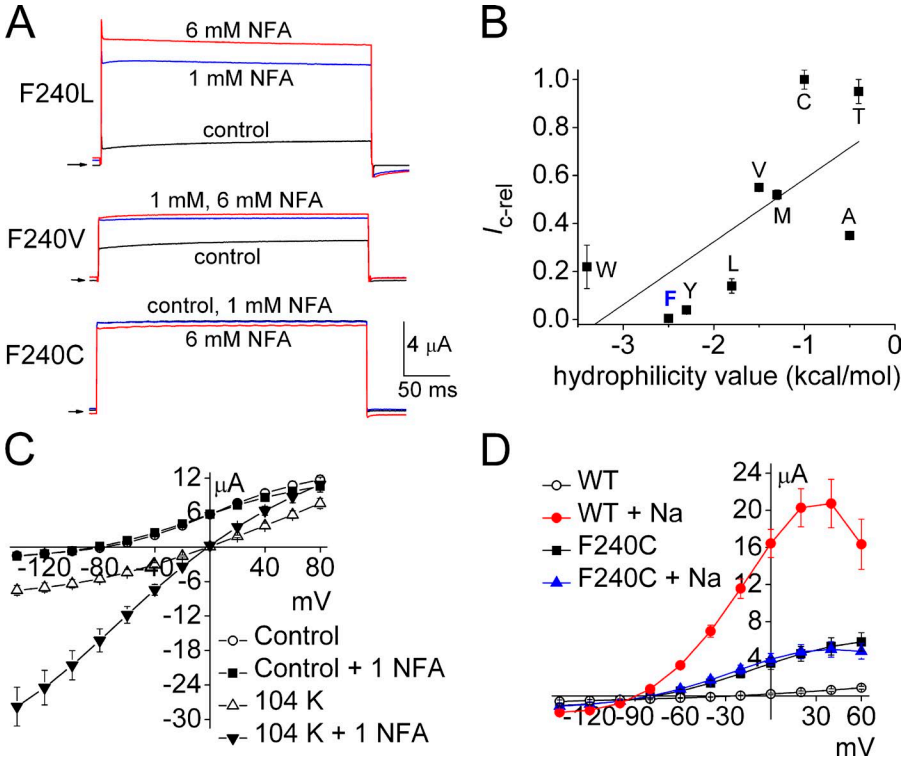

Figure 10. Substitutions of the pore helix residue Phe240 induce a spectrum of constitutive channel activity. (A) NFA further activates F240L and F240V channels, but not F240C channel currents. Currents were elicited with 300-ms pulses to 0 mV from a V_h of −80 mV. Arrows indicate 0 current level. (B) Relationship between constitutive channel activity of Phe240 mutant channels and hydrophilicity of the introduced residue (indicated by single letter code). $I_{c\text{-}rel}$ for WT ("F") and mutant channels (n = 4–12) are plotted as a function of solvent parameter (hydrophilicity) values (Levitt, 1976) for the indicated Phe240 substitution. The line represents a linear regression fit of data (adjusted R^2 = 0.41). (C) I-V_t relationships for F240C Slo2.1 channel currents measured from oocytes bathed in KCM211 or K104 extracellular solution in the absence and presence of 1 mM NFA (n = 6). (D) I-V_t relationships for WT and F240C Slo2.1 channel currents recorded before and after maximal increase in outward currents induced by NaCl loading from recording pipettes (n = 9). Error bars indicate mean ± SEM.

mutant channels. For these experiments, oocytes were injected with 10 ng of WT or mutant channel cRNA, and the I-V_t relationships in the absence and presence of 1 and 6 mM NFA were determined 3–4 d later. WT Slo2.1 channel currents were very small in the absence of NFA, increased dramatically with 1 mM NFA (Fig. 12 A), and were too large to be accurately measured at a $V_t > 0$ mV in oocytes treated with 6 mM NFA. Endogenous currents in uninjected oocytes were reduced by 1 mM NFA and increased by 6 mM NFA (Fig. 12 B). P271A channels were rescued by the second site mutations E275D (Fig. 12 C) and R190E (Fig. 12 D), but not by F240C (Fig. 12 E) or A278R (Fig. 12 F). E275A channels were rescued by A278R (Fig. 8 B), but not by R190E (Fig. 12 G) or F240C (Fig. 12 H). If F240C induces constitutive channel activity by stabilizing the selectivity filter gate in an open state, its failure to rescue the function of P271A or E275A channels implies that these later mutations prevent channel opening by inducing closure elsewhere in the ion conduction pathway. Given the location of Pro271 and Glu275, we suggest that channel closure results from an Ala substitution–induced formation of an S6 bundle crossing.

DISCUSSION

The findings presented here suggest that the structural basis of ion permeation gating in Slo2.1 K^+ channels differs from typical Kv channels. As summarized in the diagrams presented in Fig. 13, activation of Kv channels in response to membrane depolarization is mediated initially by outward displacement of the S4 segments followed by opening of the activation gate (splaying of the inner S6 segments away from the central cavity). In Slo2.1 channels, the S6 segments do not form a bundle crossing and the S4 segment is not displaced in response to voltage. Instead, the selectivity filter serves as the activation gate that is opened by an allosteric coupling mechanism initiated by intracellular Na^+ binding to the C termini.

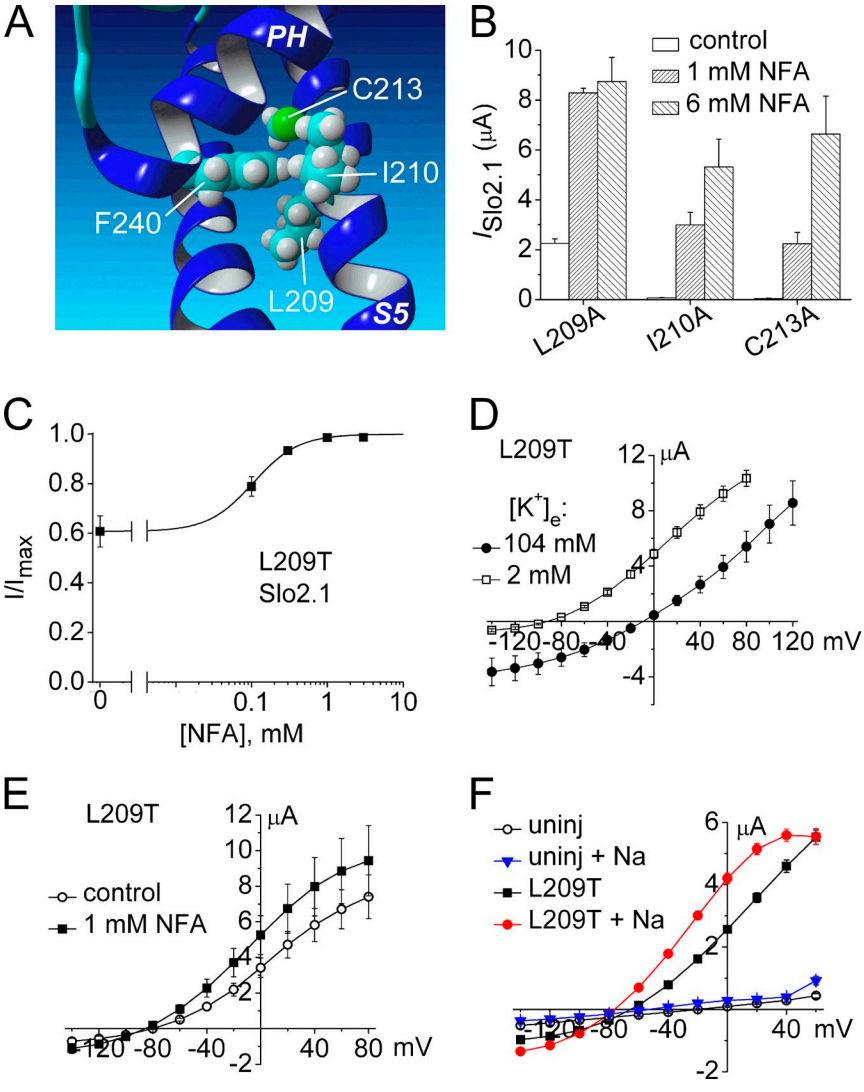

Figure 11. Mutation analysis of three residues in the S5 segment predicted to form intrasubunit interactions with the pore helix of Slo2.1. (A) MthK-based homology model of a single Slo2.1 subunit highlighting Phe240 in the pore helix (PH) and three potential interacting residues in the S5 segment. (B) Peak outward $I_{Slo2.1}$ measured at 0 mV in the absence (control) and presence of 1 and 6 mM NFA for mutant channels with indicated point mutations in S5 (n = 5–7). (C) [NFA]–response relationship for L209T Slo2.1 channels. $I_{Slo2.1}$ was measured at 0 mV and normalized to the peak current measured in the presence of 3 mM NFA. Data were fitted with a logistic equation (smooth curve). EC_{50} = 106 ± 9 μM, n_H = 1.39 ± 0.12 (n = 6). (D) I-V_t relationships for L209T $I_{Slo2.1}$ in oocytes bathed in KCM211 and K104 solutions. (E) I-V_t relations for L209T $I_{Slo2.1}$ before and after treatment with 1 mM NFA (n = 10). (F) I-V_t relationship for L209T $I_{Slo2.1}$ before and after intracellular NaCl loading. For data presented in C–F, oocytes were injected with 0.7 ng cRNA and currents were recorded 1 d later. Error bars indicate mean ± SEM.

In a typical Kv channel, the intracellular ends of the S6 segments form an intracellular activation gate that can restrict access of cytoplasmic ions and drugs to the central cavity in a voltage-dependent manner. In the closed state, the aperture formed by the S6 bundle crossing is narrow and forms a steric and hydrophobic barrier to K^+ diffusion into or out of the central cavity. In Shaker, V478 residues in S6 are located at the narrowest region of the bundle crossing, and substitution with the larger Trp causes formation of a "hydrophobic seal" (Armstrong, 2003) that strongly stabilizes the channel in a closed state (Kitaguchi et al., 2004). Only when the channel is in an open state can K^+ ions permeate the channel or charged channel blockers (e.g., quaternary ammonium compounds) applied to the intracellular solution reach their binding site within the central cavity. The phenylalkylamines verapamil and D890 are potent state-dependent blockers of L-type Ca^{2+} channels and weak blockers of delayed rectifier and Slo1 channels (Catacuzzeno et al., 1999; Harper et al., 2001). Scanning mutagenesis and functional analysis have demonstrated that these compounds can only block Ca^{2+} channels (Hescheler et al., 1982) or hERG1 K^+ channels (Zhang et al., 1999; Duan et al., 2007) that are in an open, ion-conducting state. Access of phenylalkylamines from the cytoplasm to the inner pore is prevented by the S6 bundle crossing when these channels are in a closed state. Channel opening permits access and binding of drugs to specific residues in S6 that line the central cavity (Hockerman et al., 1995, 1997; Duan et al., 2007). Although verapamil is a low-potency blocker of Slo2.1, it also interacts with residues that line the central cavity of Slo2.1. However, in contrast to voltage-dependent Ca^{2+} and Kv channels, block of Slo2.1 was not restricted to the open conducting state of the channel. Block of Slo1 by large quaternary ammonium compounds is also state independent (Li and Aldrich, 2004; Chen and Aldrich, 2011). Thus, although activation of Slo1 is highly voltage dependent compared with Slo2.1, an S6 bundle crossing does not form an intracellular gate or physical barrier to bar entry of drug molecules from the cytoplasm into the central pore in either channel type.

The voltage dependence of Slo2.1 channel activation by 1 mM NFA has a midpoint of +95 mV and is only weakly dependent on voltage (effective valence, $z = 0.48\ e$; Dai et al., 2010), which is consistent with the paucity of basic residues in the voltage sensor domain. Each S4 segment of Slo2.1 has only two basic amino acids that are balanced by the same number of acidic residues. Neutralization of all four charged residues in S4 did not alter the G-V relationship of Slo2.1 (Dai et al., 2010). Moreover, when maximally activated by high NFA, Slo2.1 currents are time independent, and channel activation is unaffected by transmembrane voltage (Dai et al., 2010). The relative unimportance of voltage in regulation of Slo2.1 gating resembles CNG channels and markedly differs from a typical Kv channel or even Slo1 channels that are strongly regulated by both $[Ca^{2+}]_i$ and voltage. However, many properties of Slo2.1

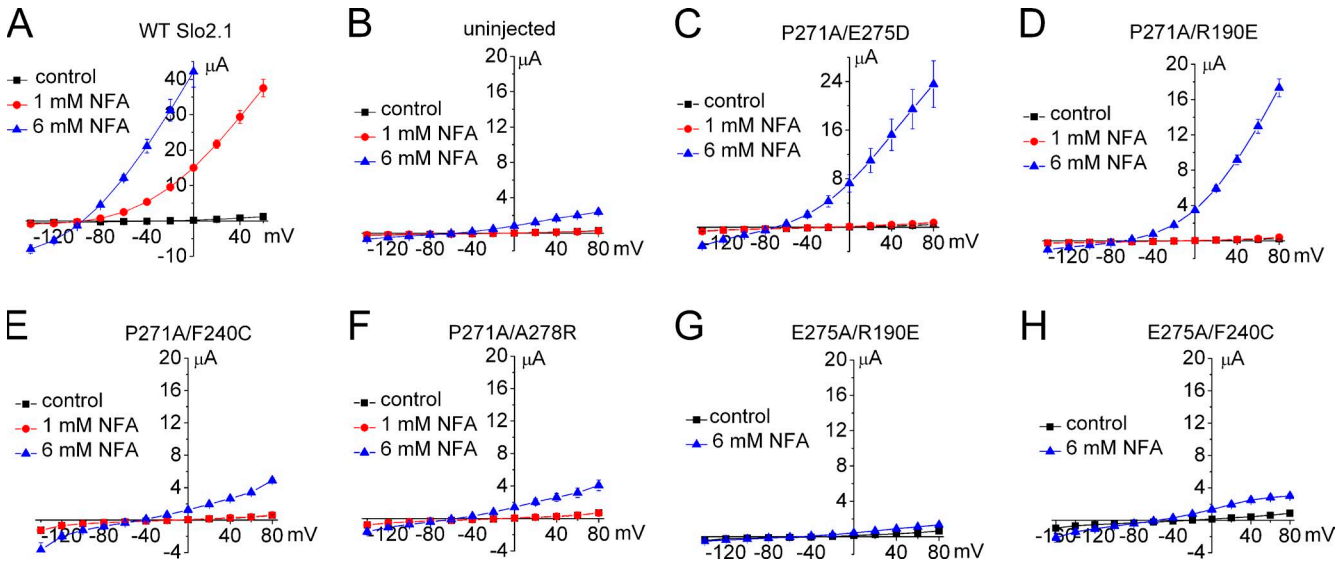

Figure 12. Screen of several gain-of-function point mutations for the ability to rescue P271A and E275A Slo2.1 channels. (A) Effect of 1 and 6 mM NFA on I-V_t relationships for oocytes expressing WT channels ($n = 4$). Oocytes were injected with 10 ng cRNA, and currents were recorded 2 d later. (B) I-V_t relationships for uninjected oocytes treated with NFA ($n = 9$). 1 mM NFA had no effect, but 6 mM NFA activated a relatively small endogenous current. (C–F) I-V_t relationships showing that E275D and R190E, but not F240C or A278R, can rescue P271A channel function ($n = 4$–7). (G and H) I-V_t relationships showing that R190E ($n = 7$) and F240C ($n = 10$) do not rescue E275A channels. For B–H, oocytes were injected with 10 ng cRNA, and currents were recorded after incubation for 2 d (C) or 3–4 d (B and D–H). Error bars indicate mean ± SEM.

gating resemble both CNG and Slo1 channels, including: (1) the fact that the S6 bundle crossing does not impede the access of large cytoplasmic molecules to the central cavity in CNG (Contreras and Holmgren, 2006) or Slo1 (Wilkens and Aldrich, 2006); (2) that seemingly subtle mutations of residues in S6 can have large effects on gating of Slo1 (Chen and Aldrich, 2011), and (3) that mutations in the pore helix (e.g., F240C in Slo2.1) can dramatically alter channel open probability of CNG channels (Contreras et al., 2008). Together these findings suggest that ligand binding to the C-terminal domain in Slo1, Slo2.1, and CNG channels cause a movement (twist?) of the S6 segments that is allosterically coupled to changes in ion permeation mediated by the selectivity filter, a structure located at the extracellular end of the ion conduction pathway. This is in contrast to Kv channels, where the S6 bundle crossing near the cytoplasmic end of the channel forms the primary activation gate, whereas a conformational change in the selectivity filter can induce "C-type" inactivation (Ogielska et al., 1995; Liu et al., 1996).

P271A channels trafficked normally to the cell surface but caused complete loss of function and could not be rescued by F240C, a second site mutation that was shown to induce constitutive activity in WT channels. Pro residues cause local distortion of α-helical geometry, and would be predicted to induce a kink in the S6 segment (Piela et al., 1987). In Slo2.1, Pro271 may cause splaying of the S6 segments away from the axis of the central pore. Mutation of Glu275 to hydrophobic residues caused complete loss of channel function, presumably by preventing ion permeation. Together with Pro271, Glu275 residues may prevent formation of the bundle crossing in Slo2.1 channels. Apparently, Glu275 is not uniquely positioned in S6 to serve this proposed role, as intragenic rescue of E275A was achieved by a second site mutation that introduced a charged residue into a position located one helical turn below Ala275 (in the E275A channel). Gating of other K^+ channels is also influenced by an acidic residue in the equivalent position to Glu275 in Slo2.1. In the closed state of MthK, Glu92 is predicted to form the narrowest region of the inner helix (TM2) bundle crossing, and its position is equivalent to Glu275 of Slo2.1 (Fig. 2 A). E92D channels gate similar to WT channels, whereas neutralization of Glu92 (E92A/Q) stabilizes the closed state of the MthK channel (Parfenova et al., 2006). In KcsA, Ala108 is located in TM2 at a position equivalent to Glu275 in Slo2.1. A108D KcsA channels have a higher open probability than WT KcsA, and the single channel conductance of mutant channels is increased up to fourfold as intracellular pH is increased (Nimigean et al., 2003). Pro475 in Shaker is equivalent to Glu275 in Slo2.1 (Fig. 2 A). P275D Shaker channels exhibit voltage-independent constitutive opening (Hackos et al., 2002). Thus, a native Glu (Glu92 in MthK, Glu275 in Slo2.1) or introduced acidic residue (A108D in KcsA, P275D in Shaker) in the equivalent position of the inner helix (TM2 or S6) enhances open probability in multiple K^+-selective channels. Substitution of other pore-lining residues in S6 with an acidic residue also induce constitutive opening of Kv channels. For example, in most Kv channels, a conserved Ala residue is located near the midpoint of each S6 segment and marks the narrowest point of the central cavity (Jiang et al., 2002). Substitution of this residue (Ala653) in hERG1 channels with an acidic (Asp, Glu) or basic (Arg, Lys) amino acid stabilizes channels in a constitutively open state (Brown

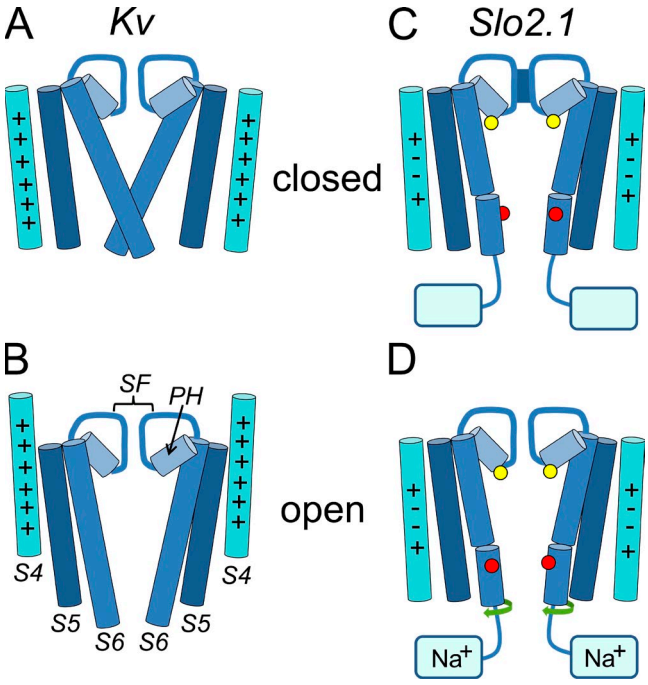

Figure 13. Diagrams illustrating the major structural changes associated with activation gating in Kv compared with changes proposed for Slo2.1 channels. (A and B) Opening of Kv channels requires a voltage-activated outward displacement of the S4 segments and splaying of the inner S6 segments (activation gate) away from the central cavity. Each panel depicts the S4-S6 segments of two diagonally positioned channel subunits. These segments, the pore helices (PH), and the selectivity filter (SF) are labeled in B. In the S4 segments, "+" indicates a basic residue. (C and D) Model of Slo2.1 channel activation. The S6 segments do not form a bundle crossing, and the S4 segments, each with an equal number of basic (+) and acidic (−) residues, do not move in response to voltage. The selectivity filter serves as the activation gate to control the transmembrane flux of K^+. Mutation of Phe240 (yellow circles, located at the base of the pore helix) to Cys induces constitutive channel opening, which suggests a key, but mechanistically undefined role for this residue in selectivity filter-mediated gating. The kink in the S6 segment of Slo2.1 represents the approximate position of Pro271 that is located four residues above Glu275 (red circles). Together these residues are proposed to prevent formation of an S6 bundle crossing in Slo2.1. Finally, it is proposed that the selectivity filter gate is allosterically activated by a twisting of S6 segments (green arrows) in response to binding of cytoplasmic Na^+ to the C termini of Slo2.1 subunits.

et al., 2008). Together these findings indicate that appropriately positioned native or introduced acidic residues within the inner helices can keep the inner bundle crossing gate in an open position in either voltage-gated or voltage-independent K^+ channels. In Kv channels, electrostatic repulsion between introduced acidic residues could cause the inner helices to splay apart and enlarge the bundle crossing aperture sufficiently to maintain the channel in an open state regardless of the position of the voltage sensors. In some voltage-independent (e.g., MthK) or weakly voltage-dependent channels (e.g., Slo2.1), the presence of acidic residues in the inner helix presumably prevents formation of the bundle crossing, and gating of ion permeation is instead controlled by the selectivity filter.

In Slo1 (BK) channels, the S6 bundle crossing undergoes a widening at the intracellular end of the channel pore upon activation, as indicated by gated access of the inactivation ball peptide (Li and Aldrich, 2006). However, the bundle crossing does not appear to gate pore access of K^+ (Li and Aldrich, 2006) or quaternary ammonium compounds (Wilkens and Aldrich, 2006) in Slo1 channels. Moreover, varying the protonation state of M314H in Slo1 caused profound changes in open probability, and M314D channels were stabilized in an open state (Chen and Aldrich, 2011). Substitution of Met314 with charged residues larger than Asp caused a less pronounced stabilization of the open state, perhaps due to electrostatic repulsion (Chen and Aldrich, 2011). Thus, subtle changes in S6 structure can markedly alter the open–closed channel state equilibrium in Slo1, similar to what we observed for the highly conserved E275D mutation in Slo2.1. The side groups of charged amino acids located in S6 prefer to be positioned in the hydrophilic environment of the pore and resist contact with the hydrophobic environment away from the pore. As proposed for CNG (Johnson and Zagotta, 2001) and Slo1 (Zhou et al., 2011) channels, if the binding of intracellular Na^+ induces a twisting motion of the C-linker and S6 segments, then perhaps the shorter side chain of Asp compared with Glu could result in the S6 segments being in a partially twisted position, intermediate between the resting (nonconducting) and fully open (conducting) state.

In summary, we propose that the general gating mechanism of Slo2.1 channels is similar to that previously described for CNG and Slo1 channels: ligand binding induces a dynamic rearrangement of the pore-lining S6 segments that allosterically induces the opening of the extracellular selectivity filter gate to permit transmembrane flux of K^+ in accordance with its electrochemical gradient.

The authors thank Li Dai, John Lahti, and Jennifer Abbruzzese for assistance with preliminary experiments.

This work was supported by grants (to M.C. Sanguinetti) from the National Institutes of Health/National Heart Lung and Blood Institute (grant R01HL103877) and from the Nora Eccles Treadwell Foundation.

Kenton J. Swartz served as editor.

Submitted: 16 July 2013
Accepted: 27 September 2013

REFERENCES

Adelman, J.P., K.Z. Shen, M.P. Kavanaugh, R.A. Warren, Y.N. Wu, A. Lagrutta, C.T. Bond, and R.A. North. 1992. Calcium-activated potassium channels expressed from cloned complementary DNAs. *Neuron.* 9:209–216. http://dx.doi.org/10.1016/0896-6273(92)90160-F

Armstrong, C.M. 2003. Voltage-gated K channels. *Sci. STKE.* 2003: re10. http://dx.doi.org/10.1126/stke.2003.188.re10

Bader, C.R., L. Bernheim, and D. Bertrand. 1985. Sodium-activated potassium current in cultured avian neurones. *Nature.* 317:540–542. http://dx.doi.org/10.1038/317540a0

Becchetti, A., and P. Roncaglia. 2000. Cyclic nucleotide-gated channels: intra- and extracellular accessibility to Cd^{2+} of substituted cysteine residues within the P-loop. *Pflugers Arch.* 440:556–565.

Bhattacharjee, A., W.J. Joiner, M. Wu, Y. Yang, F.J. Sigworth, and L.K. Kaczmarek. 2003. Slick (Slo2.1), a rapidly-gating sodium-activated potassium channel inhibited by ATP. *J. Neurosci.* 23: 11681–11691.

Brown, S., D.P. Sonntag, and M.C. Sanguinetti. 2008. A highly conserved alanine in the S6 domain of the hERG1 K^+ channel is required for normal gating. *Cell. Physiol. Biochem.* 22:601–610. http://dx.doi.org/10.1159/000185544

Bruening-Wright, A., W.S. Lee, J.P. Adelman, and J. Maylie. 2007. Evidence for a deep pore activation gate in small conductance Ca^{2+}-activated K^+ channels. *J. Gen. Physiol.* 130:601–610. http://dx.doi.org/10.1085/jgp.200709828

Budelli, G., T.A. Hage, A. Wei, P. Rojas, Y.J. Jong, K. O'Malley, and L. Salkoff. 2009. Na^+-activated K^+ channels express a large delayed outward current in neurons during normal physiology. *Nat. Neurosci.* 12:745–750. http://dx.doi.org/10.1038/nn.2313

Catacuzzeno, L., C. Trequattrini, A. Petris, and F. Franciolini. 1999. Mechanism of verapamil block of a neuronal delayed rectifier K channel: active form of the blocker and location of its binding domain. *Br. J. Pharmacol.* 126:1699–1706. http://dx.doi.org/10.1038/sj.bjp.0702477

Chen, X., and R.W. Aldrich. 2011. Charge substitution for a deep-pore residue reveals structural dynamics during BK channel gating. *J. Gen. Physiol.* 138:137–154. http://dx.doi.org/10.1085/jgp.201110632

Contreras, J.E., and M. Holmgren. 2006. Access of quaternary ammonium blockers to the internal pore of cyclic nucleotide-gated channels: implications for the location of the gate. *J. Gen. Physiol.* 127:481–494. http://dx.doi.org/10.1085/jgp.200509440

Contreras, J.E., D. Srikumar, and M. Holmgren. 2008. Gating at the selectivity filter in cyclic nucleotide-gated channels. *Proc. Natl. Acad. Sci. USA.* 105:3310–3314. http://dx.doi.org/10.1073/pnas.0709809105

Craven, K.B., N.B. Olivier, and W.N. Zagotta. 2008. C-terminal movement during gating in cyclic nucleotide-modulated channels. *J. Biol. Chem.* 283:14728–14738. http://dx.doi.org/10.1074/jbc.M710463200

Dai, L., V. Garg, and M.C. Sanguinetti. 2010. Activation of Slo2.1 channels by niflumic acid. *J. Gen. Physiol.* 135:275–295. http://dx.doi.org/10.1085/jgp.200910316

Decher, N., B. Pirard, F. Bundis, S. Peukert, K.H. Baringhaus, A.E. Busch, K. Steinmeyer, and M.C. Sanguinetti. 2004. Molecular basis for Kv1.5 channel block: conservation of drug binding sites

among voltage-gated K^+ channels. *J. Biol. Chem.* 279:394–400. http://dx.doi.org/10.1074/jbc.M307411200

DeCoursey, T.E. 1995. Mechanism of K^+ channel block by verapamil and related compounds in rat alveolar epithelial cells. *J. Gen. Physiol.* 106:745–779. http://dx.doi.org/10.1085/jgp.106.4.745

Doyle, D.A., J. Morais Cabral, R.A. Pfuetzner, A. Kuo, J.M. Gulbis, S.L. Cohen, B.T. Chait, and R. MacKinnon. 1998. The structure of the potassium channel: molecular basis of K^+ conduction and selectivity. *Science.* 280:69–77. http://dx.doi.org/10.1126/science.280.5360.69

Dryer, S.E. 1994. $Na(^+)$-activated K^+ channels: a new family of large-conductance ion channels. *Trends Neurosci.* 17:155–160. http://dx.doi.org/10.1016/0166-2236(94)90093-0

Duan, J.J., J.H. Ma, P.H. Zhang, X.P. Wang, A.R. Zou, and D.N. Tu. 2007. Verapamil blocks HERG channel by the helix residue Y652 and F656 in the S6 transmembrane domain. *Acta Pharmacol. Sin.* 28:959–967. http://dx.doi.org/10.1111/j.1745-7254.2007.00562.x

Egan, T.M., D. Dagan, J. Kupper, and I.B. Levitan. 1992. Properties and rundown of sodium-activated potassium channels in rat olfactory bulb neurons. *J. Neurosci.* 12:1964–1976.

Engelman, D.M., T.A. Steitz, and A. Goldman. 1986. Identifying nonpolar transbilayer helices in amino acid sequences of membrane proteins. *Annu. Rev. Biophys. Biophys. Chem.* 15:321–353. http://dx.doi.org/10.1146/annurev.bb.15.060186.001541

Flynn, G.E., and W.N. Zagotta. 2001. Conformational changes in S6 coupled to the opening of cyclic nucleotide-gated channels. *Neuron.* 30:689–698. http://dx.doi.org/10.1016/S0896-6273(01)00324-5

Garg, P., and M.C. Sanguinetti. 2012. Structure-activity relationship of fenamates as Slo2.1 channel activators. *Mol. Pharmacol.* 82:795–802. http://dx.doi.org/10.1124/mol.112.079194

Garg, V., F.B. Sachse, and M.C. Sanguinetti. 2012. Tuning of EAG K(+) channel inactivation: molecular determinants of amplification by mutations and a small molecule. *J. Gen. Physiol.* 140:307–324. http://dx.doi.org/10.1085/jgp.201210826

Goldin, A.L. 1991. Expression of ion channels by injection of mRNA into *Xenopus* oocytes. *Methods Cell Biol.* 36:487–509. http://dx.doi.org/10.1016/S0091-679X(08)60293-9

Hackos, D.H., T.H. Chang, and K.J. Swartz. 2002. Scanning the intracellular S6 activation gate in the shaker K^+ channel. *J. Gen. Physiol.* 119:521–532. http://dx.doi.org/10.1085/jgp.20028569

Hage, T.A., and L. Salkoff. 2012. Sodium-activated potassium channels are functionally coupled to persistent sodium currents. *J. Neurosci.* 32:2714–2721. http://dx.doi.org/10.1523/JNEUROSCI.5088-11.2012

Haimann, C., and C.R. Bader. 1989. Sodium-activated potassium channel in avian sensory neurons. *Cell Biol. Int. Rep.* 13:1133–1139. http://dx.doi.org/10.1016/0309-1651(89)90027-1

Haimann, C., L. Bernheim, D. Bertrand, and C.R. Bader. 1990. Potassium current activated by intracellular sodium in quail trigeminal ganglion neurons. *J. Gen. Physiol.* 95:961–979. http://dx.doi.org/10.1085/jgp.95.5.961

Haimann, C., J. Magistretti, and B. Pozzi. 1992. Sodium-activated potassium current in sensory neurons: a comparison of cell-attached and cell-free single-channel activities. *Pflugers Arch.* 422:287–294. http://dx.doi.org/10.1007/BF00376215

Hamill, O.P., A. Marty, E. Neher, B. Sakmann, and F.J. Sigworth. 1981. Improved patch-clamp techniques for high-resolution current recording from cells and cell-free membrane patches. *Pflugers Arch.* 391:85–100. http://dx.doi.org/10.1007/BF00656997

Harper, A.A., L. Catacuzzeno, C. Trequattrini, A. Petris, and F. Franciolini. 2001. Verapamil block of large-conductance Ca-activated K channels in rat aortic myocytes. *J. Membr. Biol.* 179:103–111. http://dx.doi.org/10.1007/s002320010041

Hescheler, J., D. Pelzer, G. Trube, and W. Trautwein. 1982. Does the organic calcium channel blocker D600 act from inside or outside on the cardiac cell membrane? *Pflugers Arch.* 393:287–291. http://dx.doi.org/10.1007/BF00581411

Hockerman, G.H., B.D. Johnson, T. Scheuer, and W.A. Catterall. 1995. Molecular determinants of high affinity phenylalkylamine block of L-type calcium channels. *J. Biol. Chem.* 270:22119–22122. http://dx.doi.org/10.1074/jbc.270.38.22119

Hockerman, G.H., B.D. Johnson, M.R. Abbott, T. Scheuer, and W.A. Catterall. 1997. Molecular determinants of high affinity phenylalkylamine block of L-type calcium channels in transmembrane segment IIIS6 and the pore region of the alpha1 subunit. *J. Biol. Chem.* 272:18759–18765. http://dx.doi.org/10.1074/jbc.272.30.18759

Jiang, Y., A. Lee, J. Chen, M. Cadene, B.T. Chait, and R. MacKinnon. 2002. The open pore conformation of potassium channels. *Nature.* 417:523–526. http://dx.doi.org/10.1038/417523a

Johnson, J.P. Jr., and W.N. Zagotta. 2001. Rotational movement during cyclic nucleotide-gated channel opening. *Nature.* 412:917–921. http://dx.doi.org/10.1038/35091089

Kameyama, M., M. Kakei, R. Sato, T. Shibasaki, H. Matsuda, and H. Irisawa. 1984. Intracellular Na^+ activates a K^+ channel in mammalian cardiac cells. *Nature.* 309:354–356. http://dx.doi.org/10.1038/309354a0

Kitaguchi, T., M. Sukhareva, and K.J. Swartz. 2004. Stabilizing the closed S6 gate in the Shaker Kv channel through modification of a hydrophobic seal. *J. Gen. Physiol.* 124:319–332. http://dx.doi.org/10.1085/jgp.200409098

Klein, H., L. Garneau, U. Banderali, M. Simoes, L. Parent, and R. Sauvé. 2007. Structural determinants of the closed KCa3.1 channel pore in relation to channel gating: results from a substituted cysteine accessibility analysis. *J. Gen. Physiol.* 129:299–315. http://dx.doi.org/10.1085/jgp.200609726

Krieger, E., G. Koraimann, and G. Vriend. 2002. Increasing the precision of comparative models with YASARA NOVA—a self-parameterizing force field. *Proteins.* 47:393–402. http://dx.doi.org/10.1002/prot.10104

Krieger, E., K. Joo, J. Lee, J. Lee, S. Raman, J. Thompson, M. Tyka, D. Baker, and K. Karplus. 2009. Improving physical realism, stereochemistry, and side-chain accuracy in homology modeling: Four approaches that performed well in CASP8. *Proteins.* 77(Suppl 9):114–122. http://dx.doi.org/10.1002/prot.22570

Kurokawa, J., S. Adachi-Akahane, and T. Nagao. 1997. 1,5-benzothiazepine binding domain is located on the extracellular side of the cardiac L-type Ca^{2+} channel. *Mol. Pharmacol.* 51:262–268.

Lee, K.S., and R.W. Tsien. 1983. Mechanism of calcium channel blockade by verapamil, D600, diltiazem and nitrendipine in single dialysed heart cells. *Nature.* 302:790–794. http://dx.doi.org/10.1038/302790a0

Levitt, M. 1976. A simplified representation of protein conformations for rapid simulation of protein folding. *J. Mol. Biol.* 104:59–107. http://dx.doi.org/10.1016/0022-2836(76)90004-8

Li, W., and R.W. Aldrich. 2004. Unique inner pore properties of BK channels revealed by quaternary ammonium block. *J. Gen. Physiol.* 124:43–57. http://dx.doi.org/10.1085/jgp.200409067

Li, W., and R.W. Aldrich. 2006. State-dependent block of BK channels by synthesized shaker ball peptides. *J. Gen. Physiol.* 128:423–441. http://dx.doi.org/10.1085/jgp.200609521

Liu, J., and S.A. Siegelbaum. 2000. Change of pore helix conformational state upon opening of cyclic nucleotide-gated channels. *Neuron.* 28:899–909. http://dx.doi.org/10.1016/S0896-6273(00)00162-8

Liu, Y., M.E. Jurman, and G. Yellen. 1996. Dynamic rearrangement of the outer mouth of a K^+ channel during gating. *Neuron.* 16:859–867. http://dx.doi.org/10.1016/S0896-6273(00)80106-3

Mitcheson, J.S., J. Chen, M. Lin, C. Culberson, and M.C. Sanguinetti. 2000. A structural basis for drug-induced long QT syndrome. *Proc. Natl. Acad. Sci. USA.* 97:12329–12333. http://dx.doi.org/10.1073/pnas.210244497

Nimigean, C.M., J.S. Chappie, and C. Miller. 2003. Electrostatic tuning of ion conductance in potassium channels. *Biochemistry.* 42:9263–9268. http://dx.doi.org/10.1021/bi0348720

Ogielska, E.M., W.N. Zagotta, T. Hoshi, S.H. Heinemann, J. Haab, and R.W. Aldrich. 1995. Cooperative subunit interactions in C-type inactivation of K channels. *Biophys. J.* 69:2449–2457. http://dx.doi.org/10.1016/S0006-3495(95)80114-1

Ottolia, M., and L. Toro. 1994. Potentiation of large conductance K_{Ca} channels by niflumic, flufenamic, and mefenamic acids. *Biophys. J.* 67:2272–2279. http://dx.doi.org/10.1016/S0006-3495(94)80712-X

Parfenova, L.V., B.M. Crane, and B.S. Rothberg. 2006. Modulation of MthK potassium channel activity at the intracellular entrance to the pore. *J. Biol. Chem.* 281:21131–21138. http://dx.doi.org/10.1074/jbc.M603109200

Piela, L., G. Némethy, and H.A. Scheraga. 1987. Proline-induced constraints in alpha-helices. *Biopolymers.* 26:1587–1600. http://dx.doi.org/10.1002/bip.360260910

Rodrigo, G.C., and R.A. Chapman. 1990. A sodium-activated potassium current in intact ventricular myocytes isolated from the guinea-pig heart. *Exp. Physiol.* 75:839–842.

Sanguinetti, M.C. 1990. Na^+-activated and ATP-sensitive K^+ channels in the heart. *In* Potassium Channels: Basic Function and Therapeutic Aspects. T. Colatsky, editor. Alan R. Liss, Inc., New York. 85–110.

Schreibmayer, W., H.A. Lester, and N. Dascal. 1994. Voltage clamping of *Xenopus laevis* oocytes utilizing agarose-cushion electrodes. *Pflugers Arch.* 426:453–458. http://dx.doi.org/10.1007/BF00388310

Stühmer, W. 1992. Electrophysiological recording from *Xenopus* oocytes. *Methods Enzymol.* 207:319–339. http://dx.doi.org/10.1016/0076-6879(92)07021-F

Sun, Z.P., M.H. Akabas, E.H. Goulding, A. Karlin, and S.A. Siegelbaum. 1996. Exposure of residues in the cyclic nucleotide-gated channel pore: P region structure and function in gating. *Neuron.* 16:141–149. http://dx.doi.org/10.1016/S0896-6273(00)80031-8

Tamsett, T.J., K.E. Picchione, and A. Bhattacharjee. 2009. NAD^+ activates K_{Na} channels in dorsal root ganglion neurons. *J. Neurosci.* 29:5127–5134. http://dx.doi.org/10.1523/JNEUROSCI.0859-09.2009

Thompson, J., and T. Begenisich. 2012. Selectivity filter gating in large-conductance $Ca(^{2+})$-activated K^+ channels. *J. Gen. Physiol.* 139:235–244. http://dx.doi.org/10.1085/jgp.201110748

Wang, Z., T. Kimitsuki, and A. Noma. 1991. Conductance properties of the $Na(^+)$-activated K^+ channel in guinea-pig ventricular cells. *J. Physiol.* 433:241–257.

Wendt-Gallitelli, M.F., T. Voigt, and G. Isenberg. 1993. Microheterogeneity of subsarcolemmal sodium gradients. Electron probe microanalysis in guinea-pig ventricular myocytes. *J. Physiol.* 472:33–44.

Wilkens, C.M., and R.W. Aldrich. 2006. State-independent block of BK channels by an intracellular quaternary ammonium. *J. Gen. Physiol.* 128:347–364. http://dx.doi.org/10.1085/jgp.200609579

Wojtovich, A.P., T.A. Sherman, S.M. Nadtochiy, W.R. Urciuoli, P.S. Brookes, and K. Nehrke. 2011. SLO-2 is cytoprotective and contributes to mitochondrial potassium transport. *PLoS ONE.* 6:e28287. http://dx.doi.org/10.1371/journal.pone.0028287

Yan, Y., Y. Yang, S. Bian, and F.J. Sigworth. 2012. Expression, purification and functional reconstitution of slack sodium-activated potassium channels. *J. Membr. Biol.* 245:667–674. http://dx.doi.org/10.1007/s00232-012-9425-7

Yuan, A., C.M. Santi, A. Wei, Z.W. Wang, K. Pollak, M. Nonet, L. Kaczmarek, C.M. Crowder, and L. Salkoff. 2003. The sodium-activated potassium channel is encoded by a member of the Slo gene family. *Neuron.* 37:765–773. http://dx.doi.org/10.1016/S0896-6273(03)00096-5

Zhainazarov, A.B., and B.W. Ache. 1997. Gating and conduction properties of a sodium-activated cation channel from lobster olfactory receptor neurons. *J. Membr. Biol.* 156:173–190. http://dx.doi.org/10.1007/s002329900199

Zhang, S., Z. Zhou, Q. Gong, J.C. Makielski, and C.T. January. 1999. Mechanism of block and identification of the verapamil binding domain to HERG potassium channels. *Circ. Res.* 84:989–998. http://dx.doi.org/10.1161/01.RES.84.9.989

Zhou, Y., X.M. Xia, and C.J. Lingle. 2011. Cysteine scanning and modification reveal major differences between BK channels and Kv channels in the inner pore region. *Proc. Natl. Acad. Sci. USA.* 108:12161–12166. http://dx.doi.org/10.1073/pnas.1104150108